MAX-PLANCK-INSTITUT FÜR PLASMAPHYSIK

GARCHING BEI MÜNCHEN

THE LOW ENERGY NEUTRAL PARTICLE ANALYZER (LENA) at W7-AS

H. Verbeek and A. Schiavi

IPP 9/103 October 1994

Die nachstehende Arbeit wurde im Rahmen des Vertrages zwischen dem Max-Planck-Institut für Plasmaphysik und der Europäischen Atomgemeinschaft über die Zusammenarbeit auf dem Gebiete der Plasmaphysik durchgeführt.

Contents

List of Figures

Fig.18: Time dependence of Γ during #23388 with increasing iota. At 0.4 s iota crosses the value of $\iota = 0.5$.

Fig.19: CX-spectra of 3 NBI heated discharges with different values of B_t started with nonresonant 900 MHz radiation.

Fig.20: Γ during #26448. 400 kW 70 GHz ECRH 0 to 0.22 s, 880 kW NBI 0.2 to 0.7 s, 720 kW 140 GHz ECRH 0.22 to 0.32 s.

Fig.21: CX-spectra of #26448 (see Fig.20) for NBI (solid line) and for NBI + 140 GHz ECRH (+++).

Fig.22: CX-spectra of #23550 at $\iota = 0.529$ (solid line) with H-mode and #23551 at $\iota = 0.534$ (dotted) with no H-mode..

Fig.23: CX-spectra of #23585 before (+++) and after (solid line) the H-mode transition.

Fig.24: Time dependence of the H_α−signals from the LENA port and the limiter and the CX-flux Γ during #23585 with a H-mode transition at 0.828 s.

Fig.25: Correlation of Γ and H_α−signal from the limiter ("halfa 3") for shot #23585 (see Figs.23,24).

Fig.26: CX-spectra during #28824 with $\iota = 0.341$, B_t =1.27 T and 840 kW NBI heating. In the lower part the time dependence of W (energy content) and the H_α−signal from the limiter are shown. The spectra are taken during the indicated times with *** 1st interv., +++ 2nd interv., and solid line 3rd interval.

Fig.27: CX-spectra of Hydrogen shots with B_t = 1.21 T and 840 kW NBI heating:

#25663, $\iota = 0.346$ H-mode?? (solid line) and #25664, $\iota = 0.361$ (dotted).

1 Abstract

A detailed documentation of the experimental arrangement of the Low Energy Neutral particle Analyzer (LENA) at W7–AS is given. The diagnostic was routinely measuring CX-fluxes and energy distributions during the period from 1992 to 94. Some typical results are reported and a phenomenological discussion of the reaction of the CX-fluxes and spectra to the variation of various plasma parameters is presented. The comparison with H_α—signals indicate whether variations of the CX-fluxes are due to changes of the wall recycling or due to alterations of the plasma profiles. T_i profiles near the edge can be determined from the LENA-spectra when the neutral atom density is simulated by the EIRENE code. For the latter to the thesis of Heinrich (1994)[1] is referred.

2 Zusammenfassung

Dieser Report enthält eine ausführliche Beschreibung der Diagnostik LENA an W7-AS. Während 1992–94 wurden routinemässig die Ladungsaustauschflüsse und —energieverteilungen gemessen. An Hand von typischen Messergebnissen wird die Reaktion der LENA-Signale auf die Variation verschiedener Plasmaparameter diskutiert. Aus dem Vergleich mit H_α—Messungen ergibt sich, ob Variationen der Ladungsaustauschflüsse durch Änderungerungen des Wandrecycling oder der Plasmaprofile verursacht werden. Aus den LENA– Spektren können T_i –Profile gewonnen werden, wozu auf die Dissertation von O.Heinrich[1] verwiesen wird.

3 Introduction

Low Energy Neutral Particle Analyzers (LENA) have been operated at IPP's ASDEX Tokamak at different toroidal locations [2]. The original goal of the measurements were the determination of the plasma-wall interaction of the low energy charge exchange (CX) neutrals i.e. the measurement of the CX-fluxes to the walls and their energy distributions. Later, by use of the Monte Carlo code EIRENE, it became possible to determine T_i profiles near the edge from the measured energy distributions [3]. Because of this capability it was decided to transfer one of the LENA apparatuses to the Stellarator W7-AS. On this occasion several improvements have been made. Especially a new data aquisition system has been developed. This report describes the present status of LENA at W7-AS and presents some results. A similar LENA has been installed recently at ASDEX-upgrade. The evaluation of T_i profiles from the LENA spectra using the EIRENE simulation of the neutral atom background is the subject of O.Heinrich's dissertation [1] and will not be discussed here. In this report a phenomenological discussion of the response of the LENA fluxes and spectra to the variation of the most important discharge parameters is presented.

4 The Principles of LENA

Apparatus

The basic principle of LENA is the same as at ASDEX [2]: The CX energy distributions are obtained from a time-of-flight (ToF) method. The CX flux from the Stellarator is chopped in bunches of 1 μs duration by a slotted cylinder mounted on a modified turbopump. After a flight path of 1.92 m the particles are counted by a detector based on secondary emission [4]. The neutrals impinge on a Cu converter electrode where they release electrons and possibly also negative ions. These are accelerated and focused by 2 additional electrodes to the entrance of an open multiplier (Johnston MM-1). The repetition frequency (given by the speed of the turbopump and the number of slits on the cylinder) is 6800/s. Fig.1 shows a schematic ground plan. LENA is mounted in the midplane of W7-AS at port 5' in sector 1. This toroidal location at Φ =349.8° is 10.2° away from the triangular plane. The line of sight is 1° off the radial direction.

Through the same port a H_α-diode is viewing the same plasma area which is seen by LENA. (Of course the H_α-light from the opposing inner wall is also seen). The signal of the H_α-diode is digitized with a sampling rate of 1 kHz and stored together with other Hα -signals. The H_α observation is usefull for the interpretation of changes in the CX fluxes and whether they are due to changes of the neutral atom density at the LENA location.

A special gas inlet at the LENA location is provided through a 10 mm bore tube which reaches to the outer wall of the vacuum vessel. With a controllable Piezo valve a small flow (- 5×10^{-3} mbl/s) of the discharge gas can be introduced.

This has two purposes: 1. it enhances the CX flux considerably without disturbing other diagnostics or the discharge control and 2. it provides a localized gas source which dominates all other recycling sources in the vicinity. This is very helpful for the EIRENE simulation of the neutral atoms for the T_i profile determination.

In the old LENA at ASDEX the start pulses were generated by a laser beam which passed the chopper cylinder at an angle to the neutral beam using a different pair of slits for the start pulse pick-up. This caused a timing jitter due to the limited accuracy of the slit spacings on the chopper cylinder. In the new LENA the timing signal is obtained from the same slit that produces the neutral particle pulse. This is done with an IR luminescence diode (Hitachi HE8807 SL) inside the chopper cylinder as an emitter and a Si-PIN diode (Hitachi HR8101) as a detector. The arrangement is shown in Fig.2.

Both the chopper slits and the stator slit are 0.15 mm wide. Opposite to each chopper slit is a 4 mm wide slit on the cylinder. The Si-PIN diode creates a triangular shaped pulse with a half width of 1μs (Fig.3). The maximum of the pulse marks the true start time. About 60 μs later a much longer trapezoedal pulse from the broad slits in the chopper cylinder is created. In the subsequent trigger pulse generator only the short pulses create output pulses ("turbo-clock pulses"), which trigger the ToF runs. The turbo-clock pulses are delayed by 1.8 μs. (This time is required to determine wether a photodiode pulse is short or long). The delay from the true start has to be measured with an oscilloscope

It is necessary to keep the detector insensitive during the open time of the slit to avoid overloading the multiplier by photoelectrons due to electromagnetic radiation from the plasma. The negative potential of the converter electrode is reduced by +800 V so that electrons and possible negative ions cannot reach the multiplier. On a turbo-clock pulse the +800 V are shut off to make the detector sensitive for the ToF measurement (60 μs). The rise time of the pulser is reduced to 1μs to avoid excessive ringing of the preamplifier.

The entrance aperture of the detector can be decreased to attenuate the multiplier countrate to $<2\times10^7$ cts/s. At higher countrates losses due to the multiplier dead time become excessive . This can occur especially at small flight times i.e. at high energies where the detection efficiency and the energy interval corresponding to the flight time interval are large.

This decreases the countrates also at low energies (long flight times) where the count rates are low anyhow. Alternatively and sacrifying high energies the trigger to the detector high voltage can be delayed. This makes the detector sensitive past the time where overloading can be expected and the low energy part of the spectra can be observed with improved statistics.

Data aquisition

A new data aquisition system in CAMAC has been developped by G.Schramm (E1). By a dual counter ('Lena-ctr.') the detector pulses are registered by a first

fast counter which is reset by an internal controller after 1μs (the dwelltime). A second counter triggered by the turbo-clock pulses counts the number of dwelltime intervals. It is reset by the controller after the preset number of dwelltimes (60 corresponds to the available flight time interval). After each dwelltime both numbers are transferred to a memory control module (Hytec MA 130), which switches to subsequent memory adresses. At W7–AS 8 memory modules (Hytec 140) are installed, which provide 8 $\times$ 128k - 10^6 channels with 16 bit storage capacity. This is enough for 16000 ToF distributions or a whole discharge with a duration of 2.4 s. The system works as a multiscaler with a dwelltime of 1 μs.

Since the chopper pump cannot be synchronized with any other clock, the times when the turbo-clock pulses occur have to be measured. With the experiment trigger a 1 MHz clock is started which serves as a reference for the turbo-clock. In a CAMAC module ('Mailbox') the times of the turbo-clock pulses are registered and by the MA 130 transferred to the memory where they are stored in the 2 channels following the ToF distributions. All individual ToF distributions with their times are stored sequentially (see Fig.4) . After each discharge the data are read by the experiment computer (μVax 300), where they can be evaluated together with the experiment parameters stored in the 'configuration file'.

Data evaluation

At first the sequentially stored data have to be rearranged in the timing information and the ToF spectra in a 2–dimensionally array. Fig.5 shows in a 3D-plot the variation of the ToF spectra during a discharge. Each curve is the mean over ~70 individual ToF spectra to smooth the rather larger statistical counting fluctuations.

It is seen from Fig.5 that the count rates decrease rapidly with increasing flight times. This has 2 reasons: 1.) the detector efficiency decreases with decreasing energies, and 2.) the energy intervals ΔE corresponding to the constant flight time interval decrease as $\Delta E \propto \frac{1}{t^3}$. The counting statistics is therefore poorest at the lowest energies. In practice this limits the measurement for Hydrogen to energies >14 eV , for Deuterium to >28 eV.

The energy distribution S(E) of the CX neutrals falling into the analyzer has theoretically the form of an integral over the line of sight:

$$S(E) \sim \int dx\, n_i(x) n_0(x) \langle \sigma_{cx} v_{rel} \rangle \frac{E^{1/2}}{T_i^{3/2}(x)} \exp\left(-E/T_i(x)\right) \times \exp\left(-\int \frac{ds}{\lambda_{tot}}\right) \quad (1)$$

According to eq.(1) the LENA spectra are the result of a complicated convolution of several physical quantities. S(E) is dependent on the profiles of $n_i(x)$, $n_e(x)$, $T_i(x)$, $T_e(x)$, and $n_0(x)$ the neutral atom density.

S(E) can be calculated from the measured ToF spectra taking into account the geometry and the detector calibration:

$$S(E) = \frac{N(t)}{\delta(E) A_c \Delta\Omega \Delta E(t) t_m} \quad (2)$$

where N(t) are the counts at time t, δ(E) the detection efficiency, A_c the area of the entrance slit, $\Delta\Omega$ the solid angle, and t_m the total measuring time.

An example of an energy distribution is shown in Fig.6. Here the errors due to the counting statistics are indicated by the bars.

In some cases it is useful to consider integral quantities [5] like the total flux

$$\Gamma = \int_{E_1}^{E_2} S(E)\, dE \quad (3)$$

or the energy flux (the first moment of the distribution)

$$P = \int_{E_1}^{E_2} E\, S(E)\, dE \quad (4)$$

and the mean energy of the CX particles

$$\langle E \rangle = P/\Gamma \quad (5)$$

For these integral quantities the counting statistics allow much better time resolution. $\Delta t < 1$ ms can be achieved. Rapid fluctuations like ELMs show up in these integrals.

Changes in $\langle E \rangle$ indicate changes in the shapes of the spectra: The more steeply the spectra rise to low energies the lower is $\langle E \rangle$. However, of course considerable changes of the shapes can occur that do'nt show up in $\langle E \rangle$.

5 Results

Sources of the neutral density

In normal operation the recycling at the wall close to the "helical edge" was identified as the dominant source of $n_0(x)$. The apparent discolored stripe at the wall due to the proximity of the helical edge passes just below the LENA port. Fig.7 shows the neutral flux Γ during shot #21176. At 0.35 s a significant minimum in Γ is visible. At this time a reciprocating probe was moved inward which intersects the plasma flow at the helical edge toroidially 77° upstream. As the probe takes up some ion flux the recycling at the wall further downstream is reduced and also n_0 at the LENA location. (LENA was the only diagnostic that was influenced by this probe).

With the exception of the cases with external gas puff (see below) we consider wall recycling as the dominant neutral source for LENA.

When a puff of the discharge gas is introduced through the LENA port the CX flux is considerable enhanced. To avoid overloading the multiplier the detector aperture has to be decreased. In Fig.8 the development of the CX flux during gas puffing is shown. The signal from the H_α−diode at the LENA location shows the same time dependence. The Piezo valve was open from 0.14 to 0.7 s with the voltage at the valve for the initial 20 ms twice as high as later to overcome sticking of the valve. Nevertheless the valve opens apparently not before 0.3 s at which time the CX flux rises steeply. The further slow increase is probably due

to the self enhancing effect by the recycling of the CX neutrals. As expected, the shapes of the spectra with and without external gas puff are very much the same.

Isotope effect

In principle the LENA cannot discriminate between neutrals of different masses since basically the quantity E/m is measured. Therefore, only those discharges where only one isotope (H or D) is dominant can be evaluated properly. After a change of the discharge gas it takes more than 100 shots before the new gas is dominant because of the recycling sources at the limiters and the wall. In Fig.9 the CX spectra of a Hydrogen and a Deuterium discharge with otherwise equal parameters are compared. The shapes of the spectra are not very different but the total flux is higher for Deuterium by a factor of 1.7. This is just the opposite behavior as at ASDEX. However, this difference is not significant considering that the history of the machine is very important for the absolute flux.

Dependence on $\langle n_e \rangle$

At ASDEX we observed that the LENA flux increased and the mean energy $\langle E \rangle$ decreased strongly with increasing the line averaged density [6][7]. Such a clear dependence cannot be observed at W7–AS. As an example Fig.10 shows the CX spectra from 70 GHz ECRH heated discharges in Hydrogen with various line integrated densities $\langle n_e \rangle = \int n\, dl$. Different from the ASDEX results is, that the spectra show maxima at low energies. The position of the maxima decreases from 90 eV for $\langle n_e \rangle = 3.2 \times 10^{18}$ m^{-2} to 50 eV for $\langle n_e \rangle = 4 \times 10^{19}$ m^{-2}. In the general shape, however, no unique tendency is visible.

With the full field B_t=2.5 T and 140 GHz ECRH higher densities can be reached as will be discussed in section 5.9. For otherwise equal plasma parameters there are no significant differences in the CX spectra for 70 and 140 GHz heating.

With neutral beam heating (NBI) even higher densities are obtained. Fig.11 shows the spectra of 3 NBI heated discharges with 1, 2, and 3 sources. In this case $\langle n_e \rangle$ could not be controlled and reached values of 5.0, 6.5, and 7.9×10^{19} m^{-2}. For these densities there is no maximum any more and the slope of the spectra increases with density.

It has been observed that in NBI heated discharges in W7–AS the density could not be increased above a certain limit by external gas puffing[8]. For such a discharge the variation of several parameters is shown in Fig.12. When the gas puff (3rd trace) is closed the line density ($\langle n_e \rangle = \int n\, dl$) and the energy content W increase. They decrease again when the gas puff is opened once more. With some delay, the CX flux Γ decreases by a factor of 0.6, when the valve is opened. The gas valve is far away from the LENA port, so a direct influence via increased local n_0 cannot be expected. The decrease of Γ is larger than that of $\langle n_e \rangle$. Therefore this can be understood as a decrease of n_i at the edge where the LENA particles originate. The mean energy $\langle E \rangle$ of the CX neutrals (bottom

trace) follows the energy content W (uppermost trace). This indicates higher T_i values at the edge when W is high.

Generally $\langle n_e \rangle$ is apparently not a good parameter for a consideration of the LENA results since it reflects only weakly changes in the edge density which is important for the low energy CX neutrals.

Dependence on the ECRH power

A strong dependence of the CX fluxes Γ on the heating power is observed. In Fig.13 Γ and $\langle E \rangle$ are shown for a discharge heated in steps by 3, 2, and 1 gyrotrons i.e. with 520, 330, and 180 kW. Γ decreases with decreasing power while $\langle E \rangle$ stays constant. The corresponding CX spectra are shifted down but their shapes do not change. The H_α—light observed at the LENA port drops by the same factor as Γ when 1 or 2 gyrotrons are switched off indicating that the recycling at the wall is likewise reduced. This reflects the fact that the particle confinement is poorer at higher heating power and more particles release recycling gas at the wall. It is interesting to note that the shapes of the spectra and therefore also $\langle E \rangle$ stay constant, indicating that n_i and T_i at the edge do not change.

ECRH modulation

For the determination of the electron heat transport heat wave experiments were performed [9]. For this purpose the ECRH was modulated with frequencies from 20 to 250 Hz and the time delay of $T_e(x)$ from the ECE signal was determined. The modulation of the ECRH power was also seen on the CX flux Γ and, less evident, also on $\langle E \rangle$. Therefore we had some hope that we could learn something on the ion transport from the delays of Γ and $\langle E \rangle$. As an example discharge #23664 is discussed, where the ECRH with 340 kW was modulated with 92 Hz and an amplitude of 100kW. Γ and $\langle E \rangle$ were calculated with a time resolution of ~1 ms. Bcause of the rather large statistical fluctuations the modulation is hardly seen directly on the signals. But using correlation technics the connection to the ECRH power can be clearly demonstrated. Fig.14 shows the autocorrelation functions of the ECRH power ("pecfi3") and Γ ("intfluss") and the crosscorrelation function of the two. The correlation reaches 0.4. The shift of the maximum from 0 gives the time delay in principle. A more accurate determination of the delay is obtained when the Fourier transforms of the signals and their correlations are considered. Using NAG routines the spectral density functions and the cross spectral density were calculated (Fig.15). It is seen that Γ (intfluss) and the cross spectral density have strong maxima at the modulation frequency. In this case the phase shift was $\Delta\phi$ =1.52 which corresponds to a time delay $\Delta t = \Delta\phi / 2\pi f = 2.6$ ms . $\langle E \rangle$ is much less correlated to the ECRH power, but the time delay can be determined as well and was found to be equal. We believe that the time delays can in principle be determined with sufficient accuracy.

A large number of shots have been investigated in this manner. The delay times varied between 1.5 and 5 ms. However, these data were not reproducible at all and no dependence on any discharge parameter could be found. We checked the LENA timing system carefully by comparing it with other time standards. The errors were within 1μs and no jitter in the triggers could be found. Apparently there are differences in the time bases of different diagnostics, which has been detected earlier by other diagnostics. Unfortunately we found no way to detect these.

Recycling studies

The total CX flux Γ depends strongly on the wall conditions. After glow discharge cleaning or after a new boronization Γ increases considerably during a series of equal discharges. After 26 shots 0.3 s long Γ increased by a factor of 1.2. Γ is generally twice as large for boronized walls compared to glow discharge cleaned walls without boron. Hydrogen is implanted into the surface of the walls during dicharges. With increasing saturation the recycling factor increases which means increased neutral density and increased CX fluxes.

For different wall conditions the recycling at the walls has been investigated [10]. In a series of shots $\langle n_e \rangle$ was ramped up by the external gas feed to a certain equilibrium value. Thereafter the gas feed was turned off and the decay of $\langle n_e \rangle$ was observed. Also the decay of the CX flux Γ and the mean energy $\langle E \rangle$ was measured. While $\langle n_e \rangle$ decreases exponential with increasing time constants the decay of Γ is more complicated. An example is shown in Fig.16 (#23231). The decay starts after a delay of 50 ms and it not exponential. The delay increases with increasing plateau density. The delay can be due to a change in the density profile during the decay. Langmuir probe data show that the density in the SOL decays much slower than the central density (Grigull 93).

In this context it is interesting to estimate the total particle loss by charge exchange. It is known that the vast majority of CX particles fall into the LENA energy range. Assuming that Γ as measured at the present LENA location is representative for the whole machine and the angular distribution is cosine the total CX flux to the walls can be estimated. Of course a much higher CX flux exists in the vicinity of the limiters. For shot #22810 with $\langle n_e \rangle$ =4.5$\times 10^{18}$ m^{-2} the flux to the walls (excluding the limiters) is -5.4$\times 10^{19}$ particles /s. For this shot the total particle content of 1.5$\times 10^{20}$ particles is lost by charge exchange to the walls in 3 s, which has to be replaced by -1/10 of the external gas flux.

In principle it is possible to construct the distribution of n_0 over the whole torus using a neutral gas code and the observation of H_α [11]. If one assumes that the CX flux is proportional to the local n_0 and the n_0 profiles are equal it is possible to construct the CX flux distribution over the whole stellarator, probably with the exception of the limiter region. This would yield total fluxes and also the impurity influx due to CX neutral sputtering[12].

Dependence on iota ι

In a series of equal discharges the rotational transform ι was scanned in small steps around ι = 1/2 and ι =1/3. Fig17 shows the variation of the CX flux Γ with ι. There is an apparent maximum at ι = 0.5. The minimum at ι = 0.52 corresponds to "optimum confinement". There are very little variations seen in $\langle E \rangle$, indicating that no changes in the spectrum shapes occur. Thus the variation is mainly due to changes in the recycling at the wall which varies as the particle confinement. The variations of Γ are less pronounced in the vicinity of ι = 1/3.

In Fig.18 the time development of Γ and $\langle E \rangle$ during shot #23388 are shown where the bootstrap currents were not compensated. This resulted in a slow increase of ι during the shot. At the very time t = 0.4 s when ι = 0.5 was exceeded Γ jumps up to a value 1.5 times as high and decreases again slightly while ι is increasing further. No reaction of $\langle E \rangle$ is observed.

NBI heating

Normally a target plasma produced by ECRH is used which can be maintained and heated by neutral beam injection (NBI). Due to beam fuelling density control is no longer possible in most cases. Therefore rather high densities are reached. Examples for CX spectra for different beam powers are already given in Fig.11.

NBI heated discharges can also be started successfully by nonresonant 900 MHz radiation through a special antenna (Ballico). In these cases the toroidal field strength could be chosen freely. In Fig.19 CX spectra for 3 different B_t values are shown. For these shots $\langle n_e \rangle$ were equal but the energy contents W were different. The reasons for the different spectra are not obvious so far.

Density control during NBI can be achieved when ECRH with 70 or 140 GHz is injected simultaneously. In Fig.20 the time development of of the CX flux during shot #26448 is shown, which was started with 400 kW ECRH at 70 GHz until 0.22 s. From 0.2 to 0.7 s NBI with 880 kW was on. From O.22 to 0.32 s 140 GHz ECRH with 720 kW was active. A huge increase of Γ within -20 ms occurs during the time when both NBI and 140 GHz were on. It is remarkable that the H_α—light signal from the LENA port shows only a little reaction. It is seen from Fig.21 that the CX spectra for NBI alone (solid line) and with additional ECRH (+++) have not only different heights but also shapes. This indicates large differences in the profiles of n_i and T_i. A full interpretation requires the EIRENE simulation, however.

H-mode operation

Under cartain discharge conditions a H-mode occurs at W7–AS [13][14]. It was discovered in 140 GHz ECRH heated discharges with full field (B_t=2.5 T) in a narrow range of iota above ι = 0.5. The shapes of the LENA spectra are very different when the H-mode occurs [15]. An example is shown in Fig.22. Characteristic for the H-mode (#23550 with ι = 0.529) is the steep rise at low

energies below 60 eV. This characteristic shape was also seen at spectra from the ASDEX H-mode. It was connected to a steep rise of the T_i profile at the edge [16]. Also at the JFT-2M Tokamak similar changes of the low energy neutral spectra have been observed [17]. For comparison a spectrum from a discharge with no H-mode (#23551 with ι = 0.534) is given in Fig.22. The characteristic H-mode features have been seen in many shots. A further example is shown in Fig.23 where the spectra before (+++) and after the H-mode transition are given.

The development of the total CX flux Γ and two H_α—signals for the same shot are shown in Fig.24. The characteristic drop of the H_α signal at the limiter is indicative for the H-mode. It shows also the ELMs as spikes during the H-mode. H_α observed at the LENA port shows only a very slight drop upon the H-mode transition and a recovery after ~50 ms. The same holds for Γ , but here the ELMs are seen as an increased fluctuation level. That the ELMs show up in Γ is clearly seen in Fig.25 were the crosscorrelation with the $H_\alpha$signal from the limiter is shown. The apparent delay turned out not to be real because of timing problems (see 5.5).

Recently the H-mode has also been detected in NBI heated discharges in the iota range of ι = 1/3. In Fig.26 the CX spectra during 3 phases of shot #28824 are shown. The spectra given by the solid line and the crosses show clearly the characteristic shape of H-mode spectra, which was identified for these times from the behavior of other diagnostics. But the spectrum with ***taken earlier in the discharge before the H-mode transition shows, not so clearly but visible, also the features of the H-mode transition.

A more questionable case of a H-mode shows Fig.27. These shots were NBI heated Deuterium discharges. During #25663 with ι = 0.346 some kind of transition with increased energy content occurs which is not the case in #25664 with ι = 0.361. For #25663 the CX spectrum shows clearly the characteristic H-mode shape, while #25664 has a "normal" spectrum.

A discussion of the spectra needs the EIRENE simulation for which to Heinrich's thesis (1994) [1] is referred.

Conclusions

LENA was monitoring almost every discharge during 1992 to 94. The measured low energy CX-fluxes are very sensitive to changes in the recycling. More interesting are changes of the shapes of the energy distributions due to changes of the n_i and T_i profiles at the edge. The complex nature of the LENA signals, however, makes a routine interpretation difficult.

To stimulate discussions some results are presented which show the dependence of the CX-fluxes and spectra on various plasma parameters.

A detailed evaluation requires the simulation of the neutral atom density by the EIRENE code, which is available only for selected discharges. This can lead to a better understanding of the influence of edge profiles on the bulk plasma.

Bibliography

[1] O. Heinrich, *{CX}-Ionentemperaturen in der Plasmarandschicht von {ASDEX} und W7–{AS}*, PhD thesis, TUM München, 1994.

[2] H. Verbeek, A low energy neutral particle analyzer for plasma experiments, J.Phys. E: Sci.Instrum. **19**, 964–970 (1986).

[3] H. Verbeek, O. Heinrich, R. Schneider, H. Fahrbach, W. Herrmann, J. Neuhauser, U. Stroht, D. Reiter, and the ASDEX team, Ion temperature profiles from the plasma center to the edge of {ASDEX} combining high and low energy {CX}-diagnostics, J.Nucl. Mat. **196–198**, 1027–1031 (1992).

[4] H. Verbeek and W. Eckstein, An apparatus for the production of a neutral Hydrogen beam in the energy range of 10 to 1000 eV, Technical Report 9/45, IPP, 1983.

[5] V. Dose and H. Verbeek, On-line plasma diagnostic by neutral atom time of flight analysis, Appl.Phys.Lett. **51**, 229–231 (1987).

[6] H. Verbeek, V. Dose, J.-K. Fu, and the ASDEX team, The low energy neutral fluxes and their impurity production at the walls of {ASDEX}, J.Nucl.Mat. **162–164**, 557–561 (1989).

[7] H. Verbeek and the ASEX team, Observations with the Low Energy Neutral Analyser ({LENA}) on {ASDEX}, Technical Report 9/84, IPP, 1991.

[8] A. Stäbler, R. Burhenn, P. Grigull, the ASDEX team, and the W7-AS team, Comparison of density limit physics on the {ASDEX} tokamak and the Wendelstein7–{AS} stellarator, Plasma Phys.Contr.Nucl. Fusion Research **IAEA-CN–56 vol.II**, 523–529 (1992).

[9] L. Giannone, V. Erckmann, U. Gasparino, H. Hartfuss, G. Kühner, H. Maasberg, U. Stroth, M. Tutter, and the W7-AS team, Electron thermal conductivity from heat wave propagation in Wendelstein 7–{AS}, Nucl. Fusion **32**, 1985–1999 (1992).

[10]R. Brakel and the W7-AS team, Recycling studies in the Wendelstein7–{AS} Stellarator, in *Stellarators and other helical confinement systems*, edited by IAEA, IAEA technical commitee meeting Garching, 1993.

[11]F. Sardei, H. Ringler, P. Grigull, A. Dodhy, G. Kühner, H. Maasberg, F. Penningsfeld, and the W7-AS team, Particle transport and plasma edge behaviour in the W7–{AS} stellarator, Europhys.Conf.Abstr. (15C II), 193–196 (1991).

[12]R. Behrisch, J. Roth, G. Staudenmaier, and H. Verbeek, Sputtering in fusion devices, Nucl. Instr.Meth. in Phys.Res. **B18**, 629–638 (1987).

[13]V. Erckmann, R. Brakel, R. Burhenn, P. Grigull, H. Hartfuss, J. Hofmann, R. Jänicke, H. Maasberg, H. Niedermeyer, W. Ohlendorf, H. Ringler,

A. Rudyj, F. Wagner, A. Weller, and the W7-AS team, H-mode like transitions in the W7–{AS} Stellarator with high power 140 {GH}z {ECRH}, Plasma Phys.Contr.Nucl. Fusion Research **IAEA-CN–56** (1992).

[14]V. Erckmann, F. Wagner, et al., H mode of the W7–{AS} Stellarator, Phys.Rev.Lett. **70**, 2086–2089 (1993).

[15]H. Verbeek, O. Heinrich, and the W7-AS team, Low energy neutral particle analysis at the Stellarator W7–{AS}, Europhys. Conf. Abstr. **17C pt.II**, 727–730 (1993).

[16]R. Schneider, H. Verbeek, D. Reiter, J. Neuhauser, and the ASDEX team, Ion temperature near the separatrix at {ASDEX}, Europhys. Conf.Abstr. **15C III**, 117–120 (1991).

[17]Y. Miura, F. Okano, N. Suzuki, M. Mori, et al., Rapid Change of Hydrogen Neutral Energy Distribution at L/H-Transition in {JFT}-2M H-mode, Technical Report NIFS-134, NIFS Nagoya, 1992.

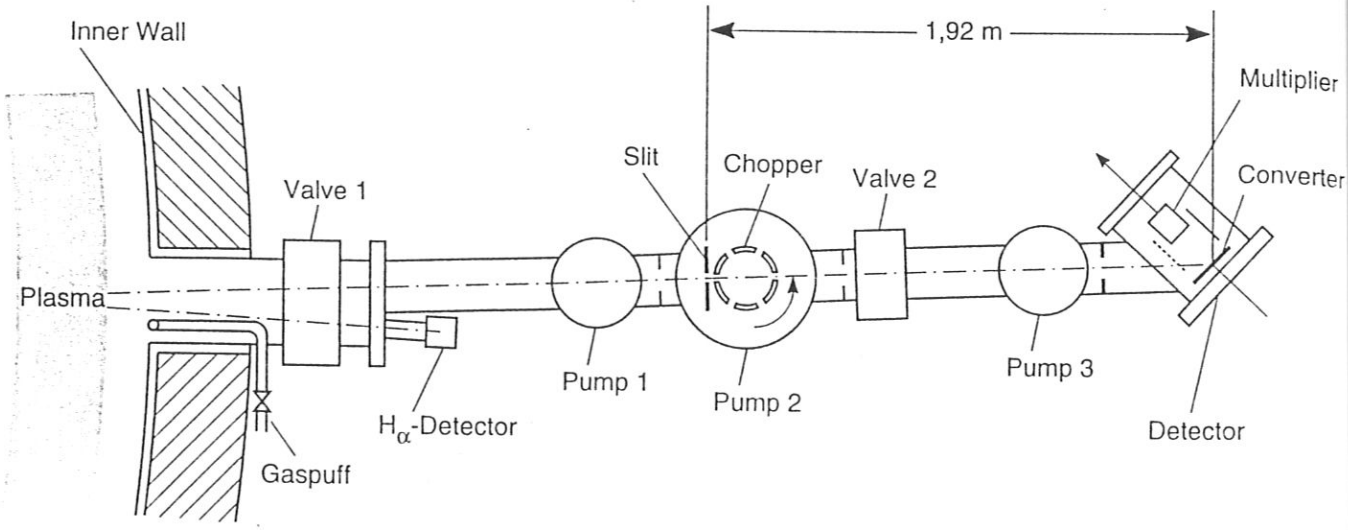

Fig.1: Schematic ground plan of LENA.

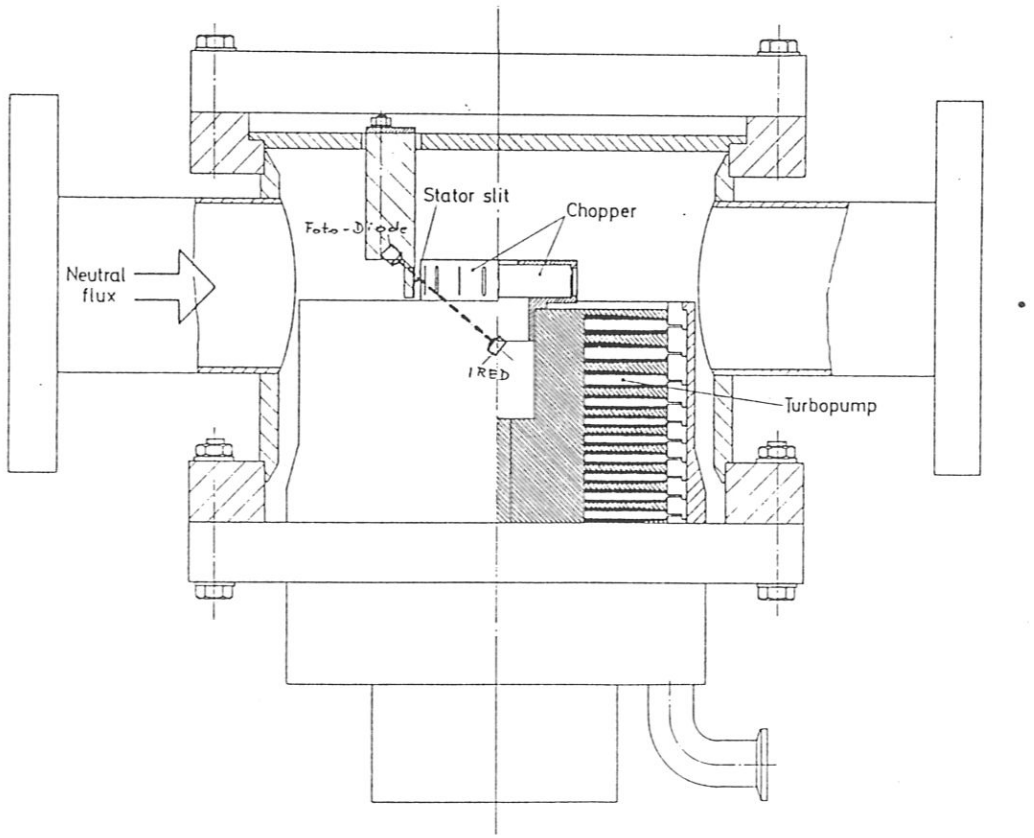

Fig.2: The chopper with the start pulse generator.

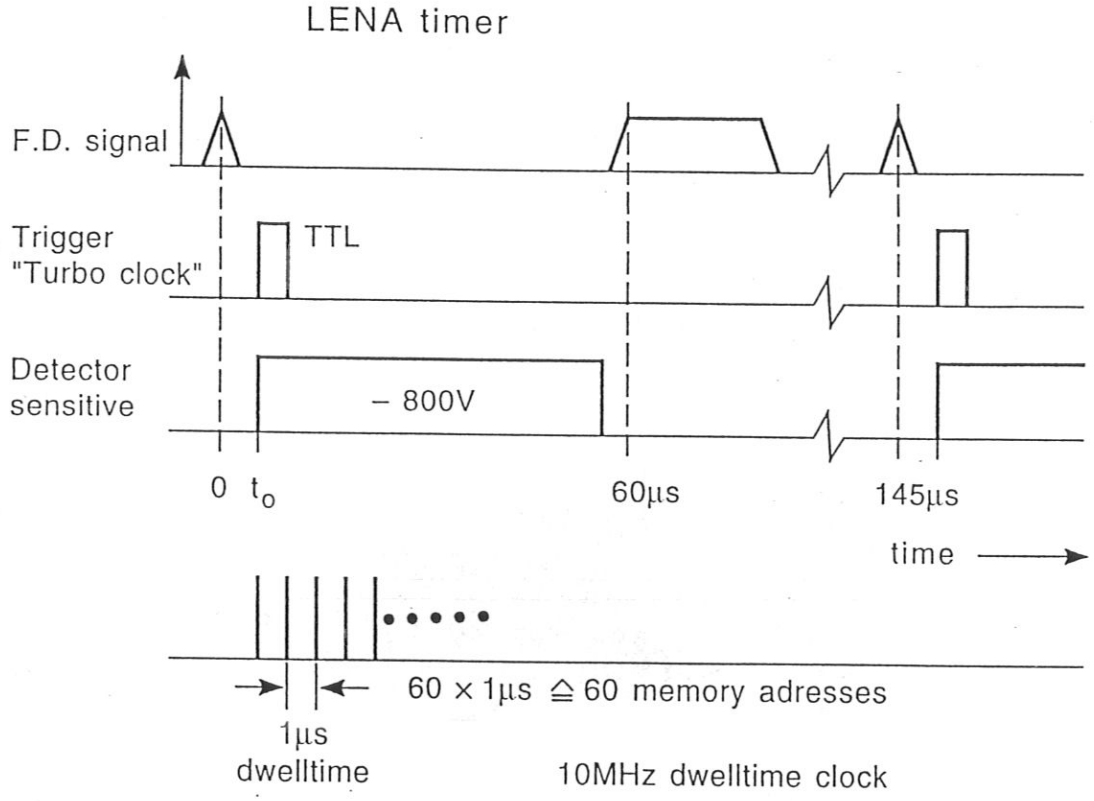

Fig.3: Timing of the LENA.

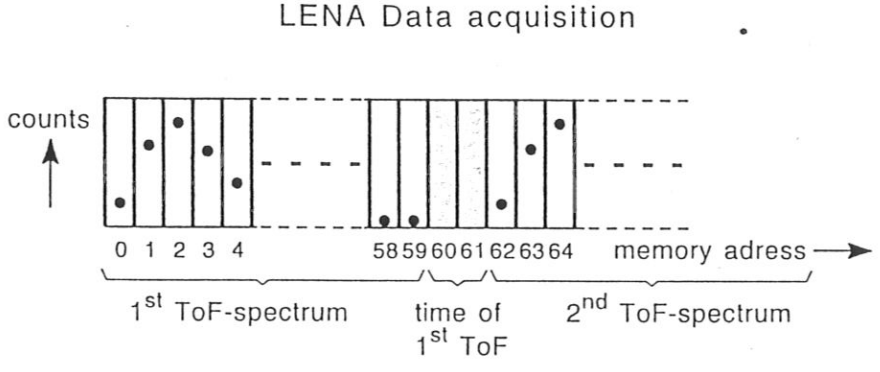

Fig.4: LENA data aquisition.

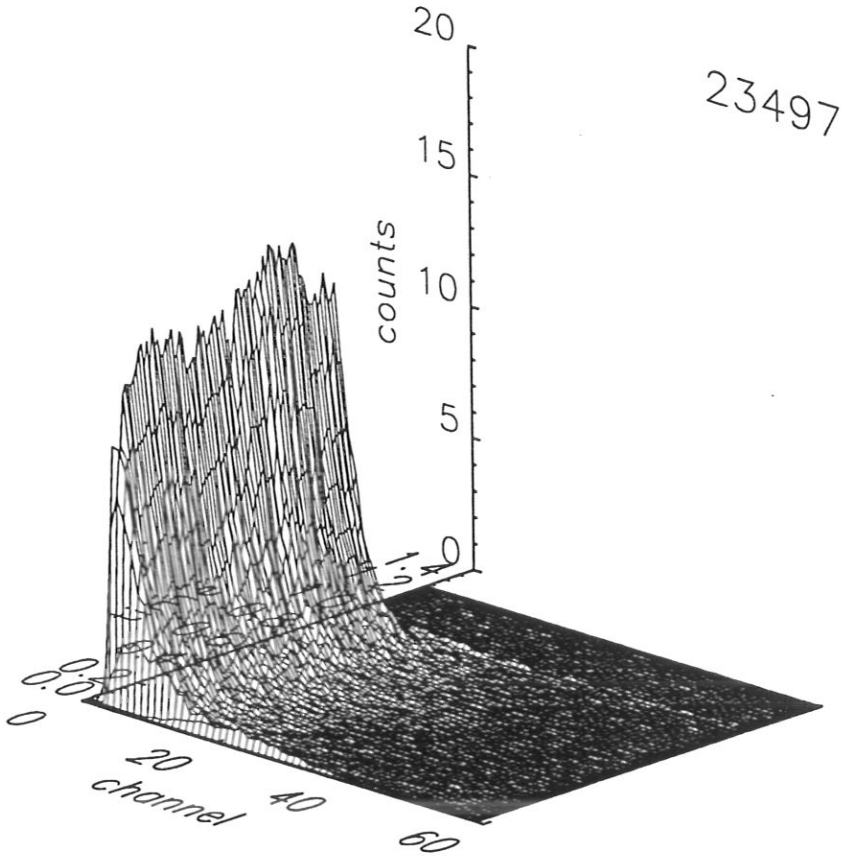

Fig.5: Development of the ToF—distributions during #23497. The channel nr. corresponds to the flight time in μs.

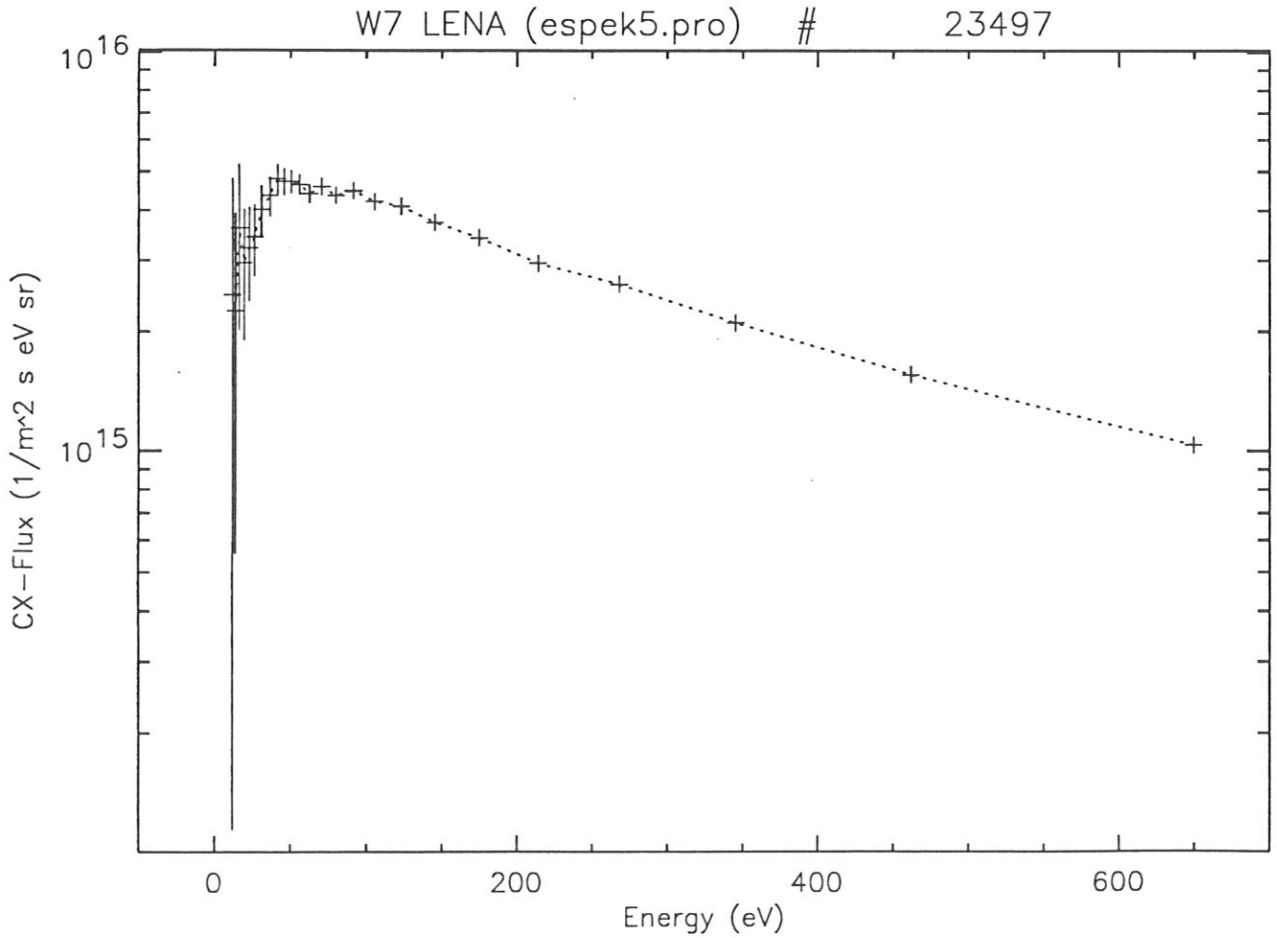

Fig.6: Energy distribution of the CX neutrals averaged over the time interval from 0.15 to 0.3 s of #23497 as in Fig.5.

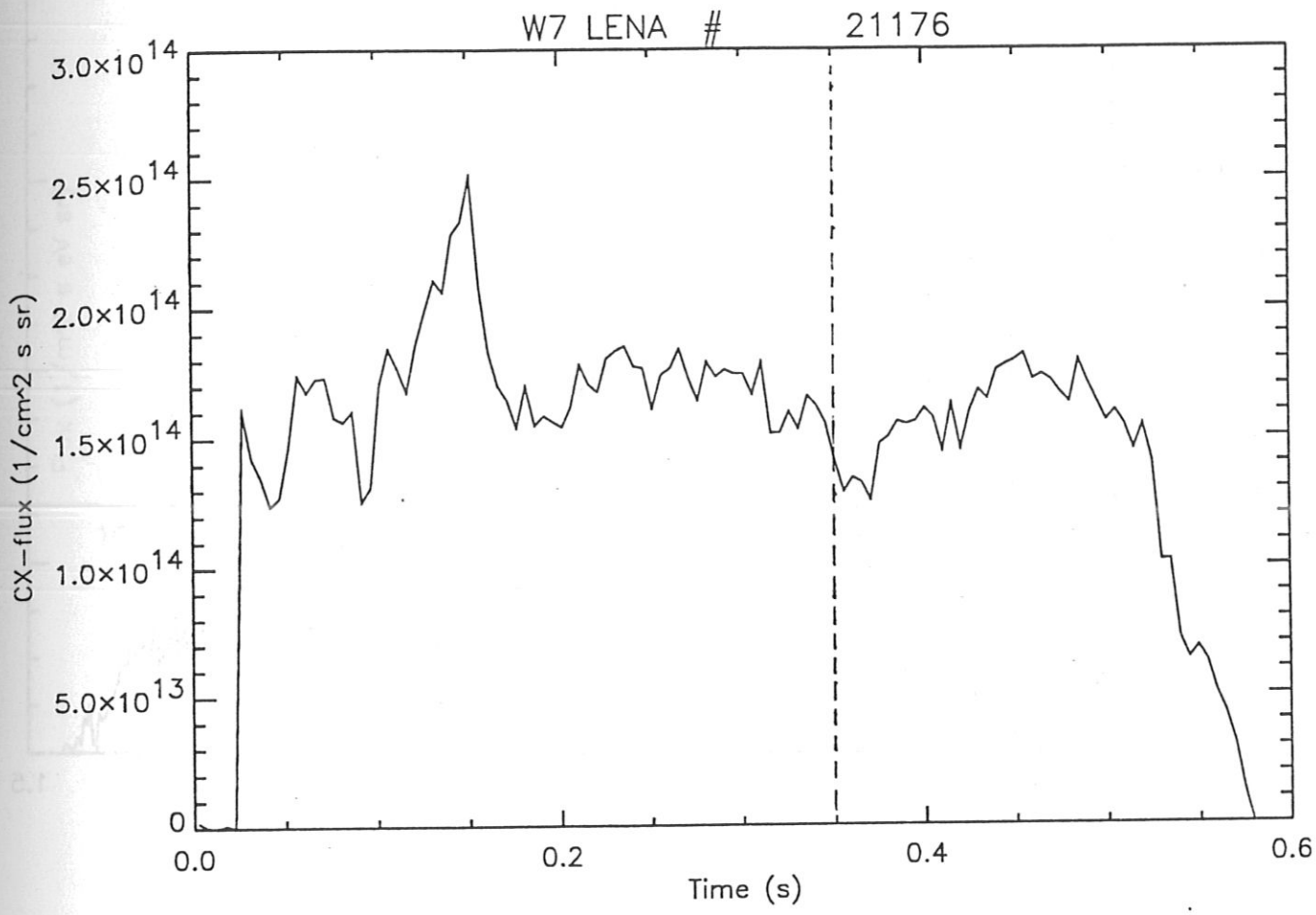

Fig.7: The CX-flux Γ during #21176. At 0.35 s a reciprocating probe was moved into the plasma edge.

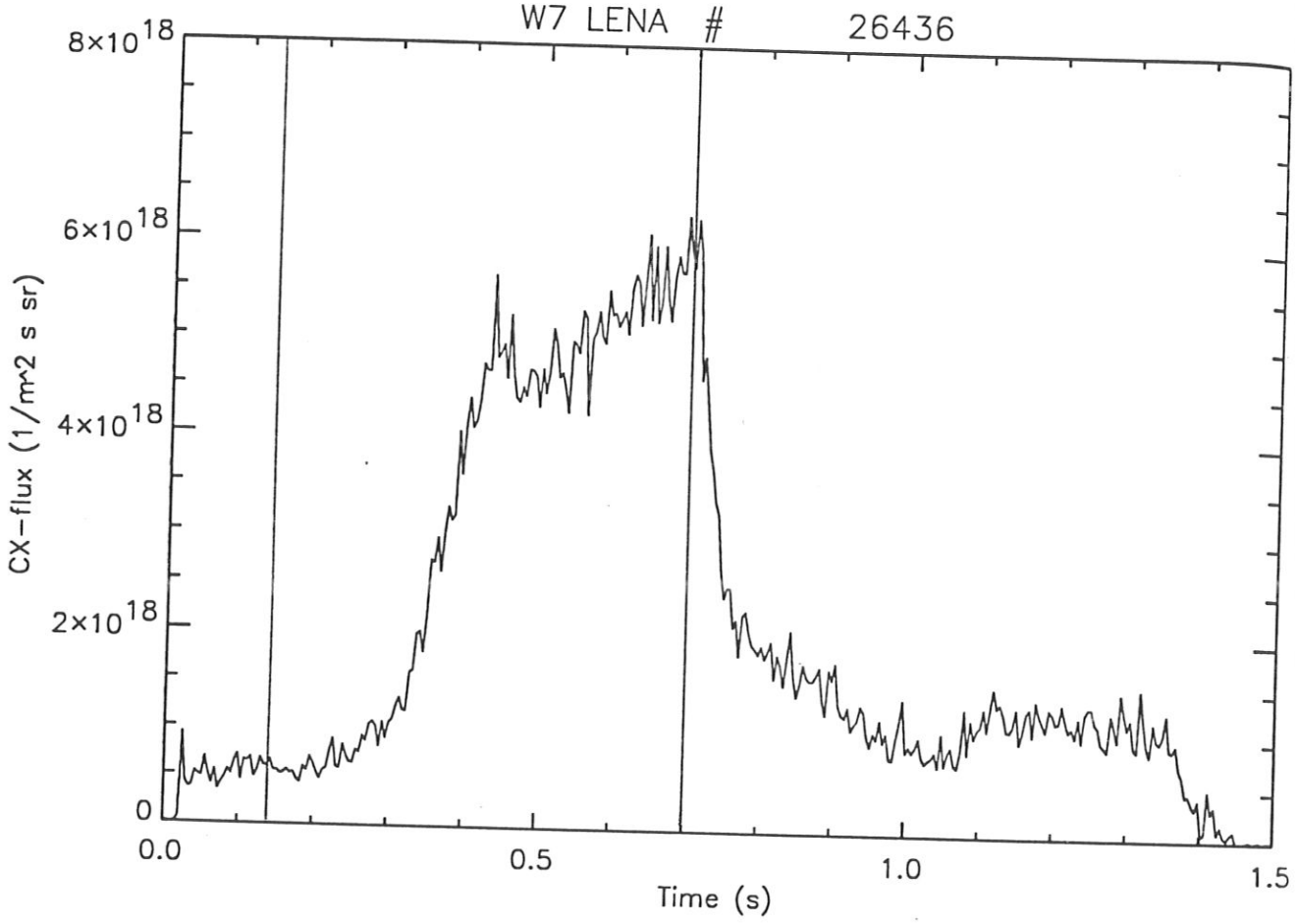

Fig.8 : The CX-flux Γduring #26436. From 0.3 to 0.7 s the external gas puff at the LENA port was open.

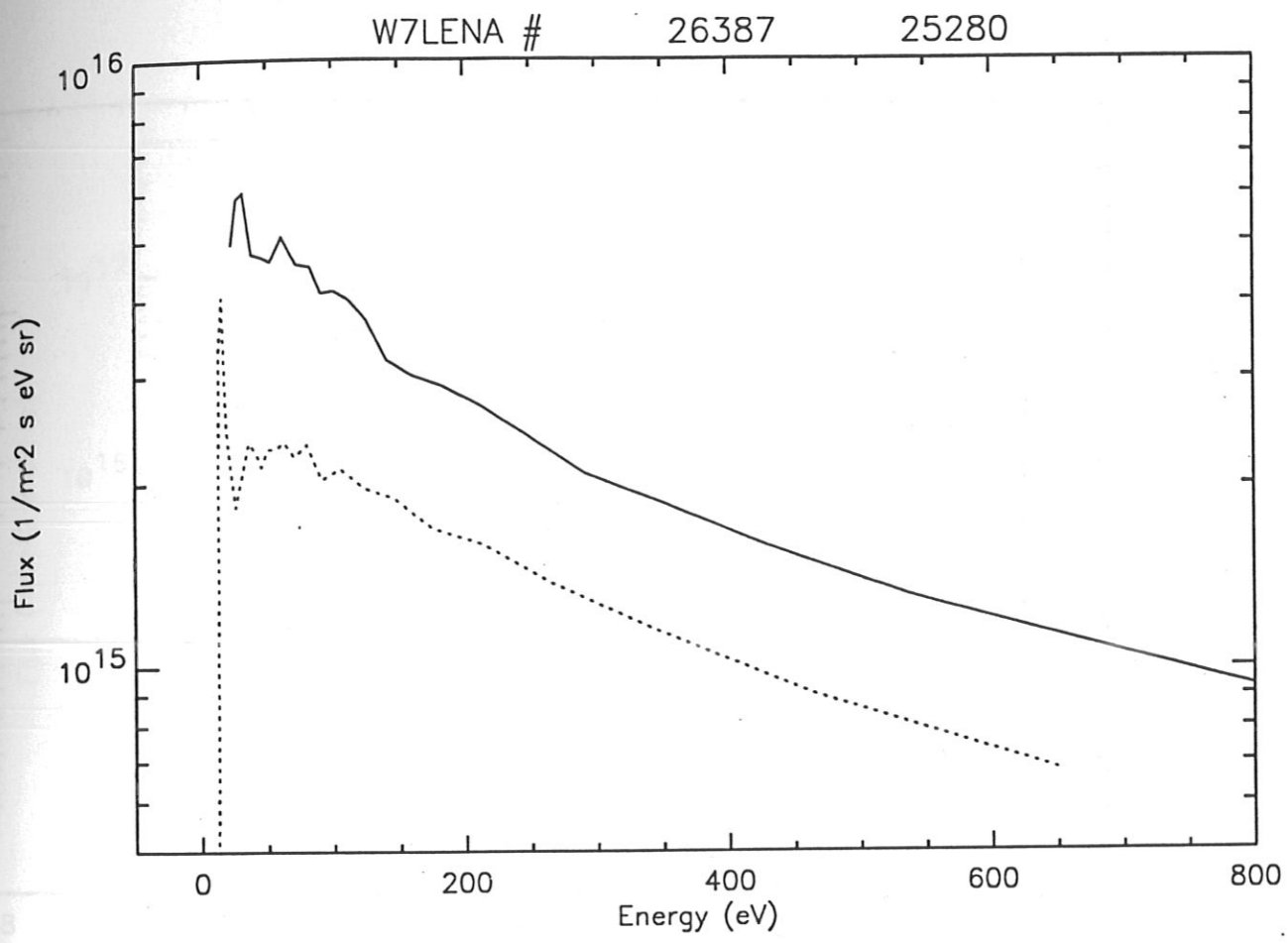

Fig.9: Comparison of the CX-spectra for discharges in Hydrogen (dotted) and Deuterium (solid).

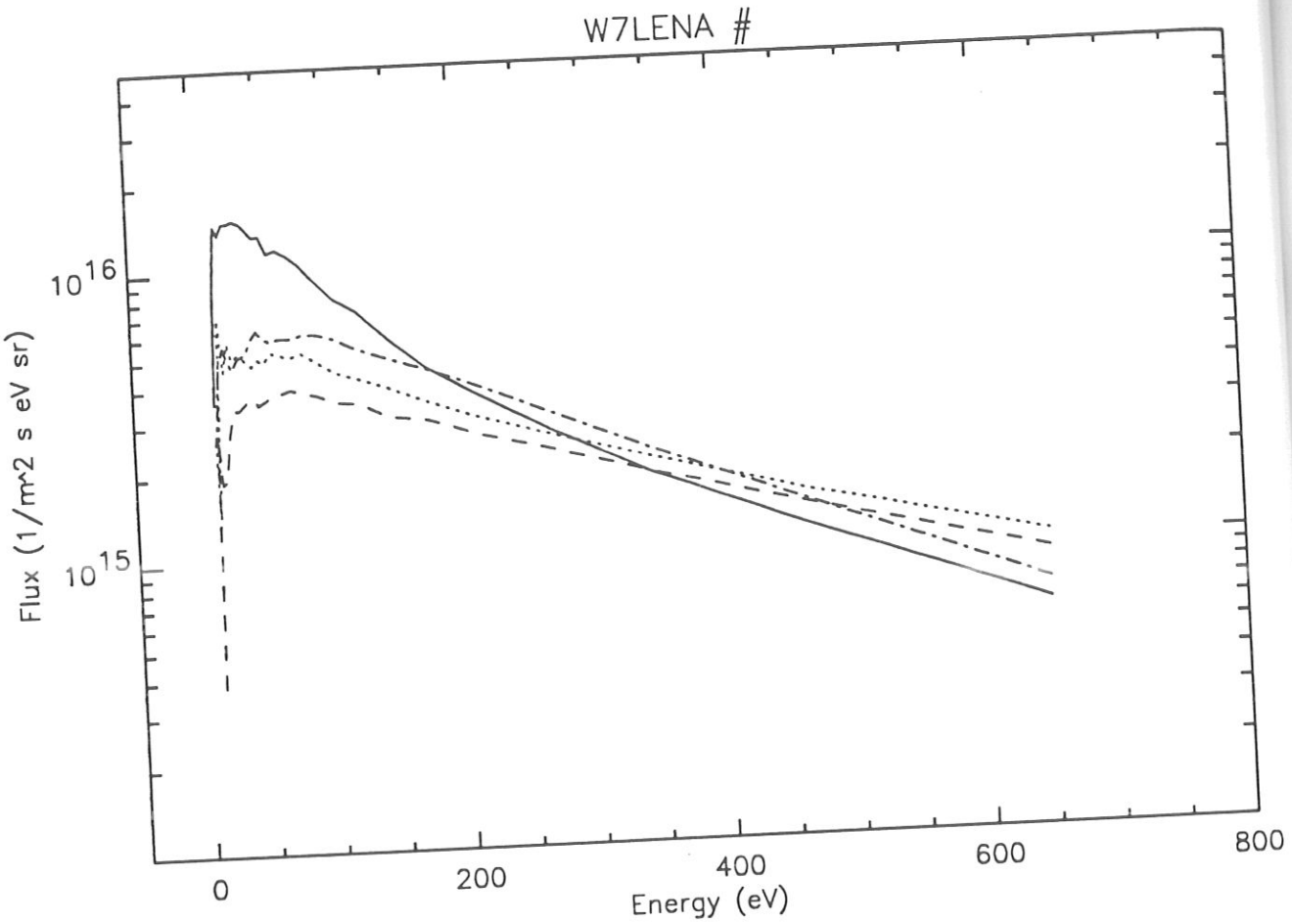

Fig.10: CX-spectra of Hydrogen discharges with ι = 0.525, B_t = 2.5 T, 400 kW ECRH-heating, and various densities $\langle n_e \rangle$ (in units of $10^{19}\mathrm{m}^{-2}$)

$\langle n_e \rangle$ = 4.0 ,#23594 (solid)

$\langle n_e \rangle$ = 1.4 ,#23007 (dotted)

$\langle n_e \rangle$ = 0.68 ,#22994 (dashed)

$\langle n_e \rangle$ = 0.32 ,#23004 (dash-dot).

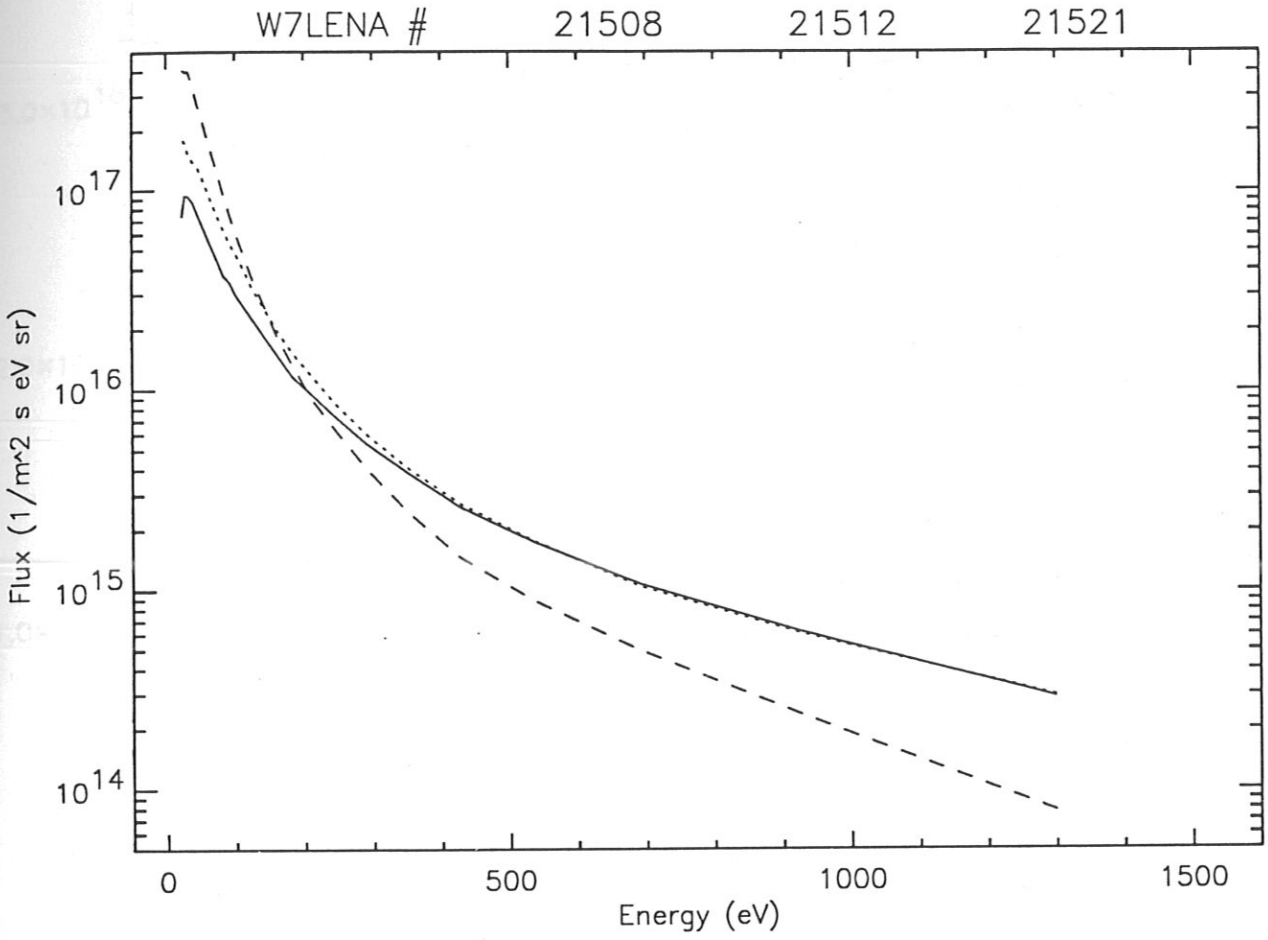

Fig.11: CX-spectra of deuterium discharges with ι =0.328 and NBI heating with powers:

P_1 = 0.42 MW (1 source) , #21508 (solid)

P_2 = 0.85 MW (2 sources) , #21512 (dotted)

P_3 = 1.28 MW (3 sources) , #21521 (dashed)

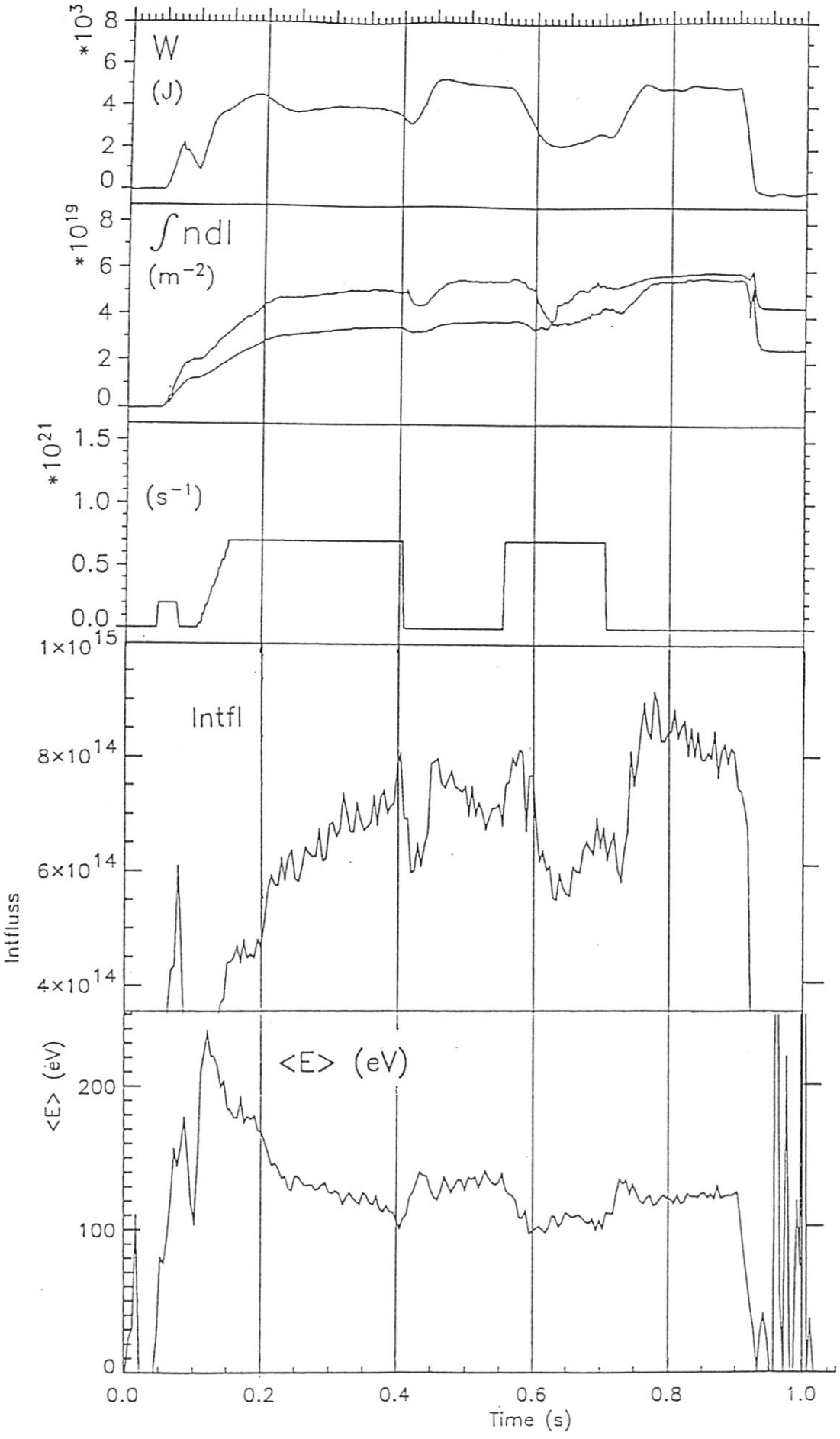

Fig.12: Time development of #21467 heated by 450 kW NBI. From top: W, total energy content; $\langle n_e \rangle = \int n\, dl$ for 2 lines of sight; the external gas feed; CX-flux Γ ("intfluss") and $\langle E \rangle$ of the CX-neutrals.

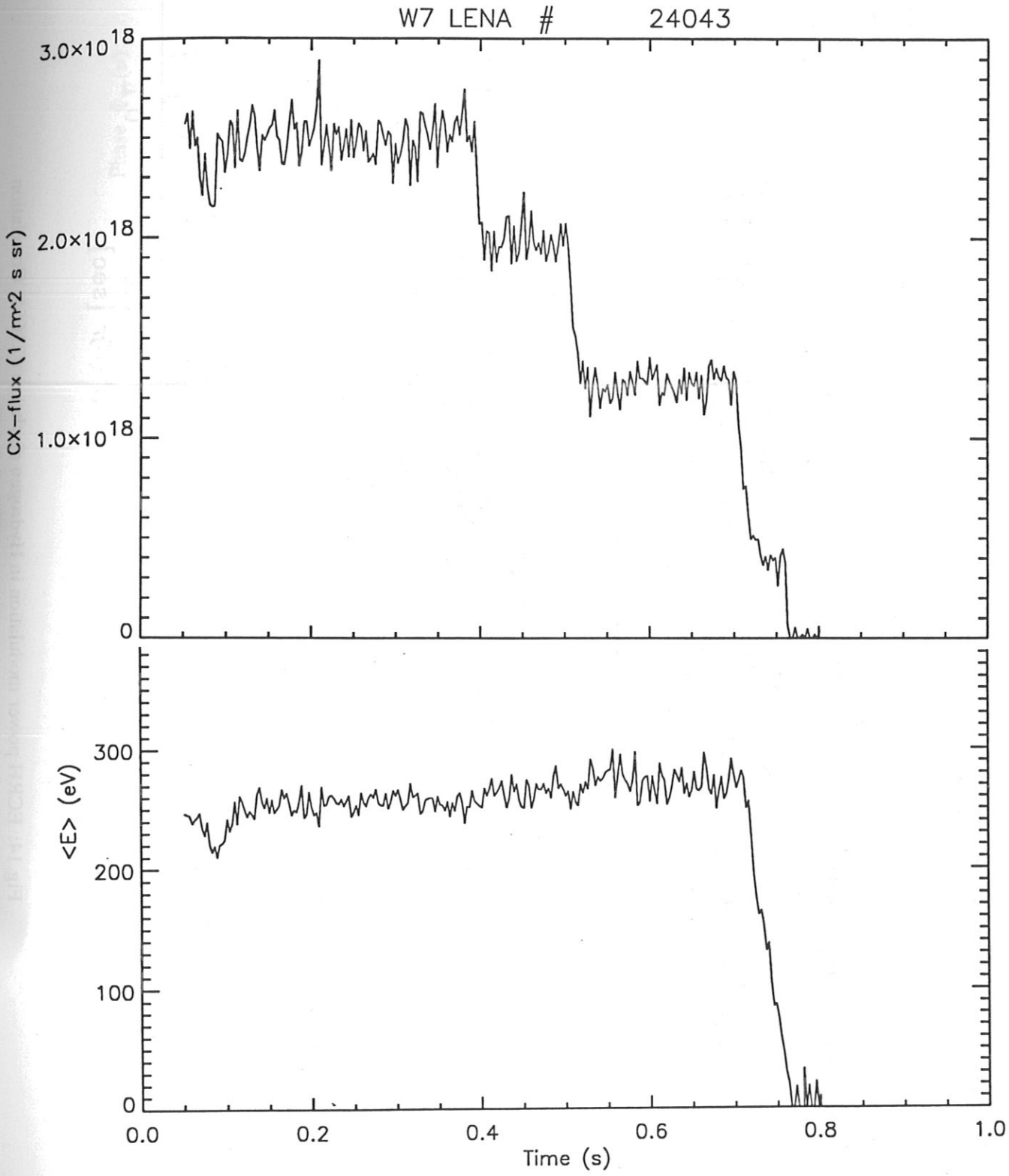

Fig.13: Time dependence of Γ and $\langle E \rangle$ for #24043 heated with 3, 2, and 1 gyrotrons.

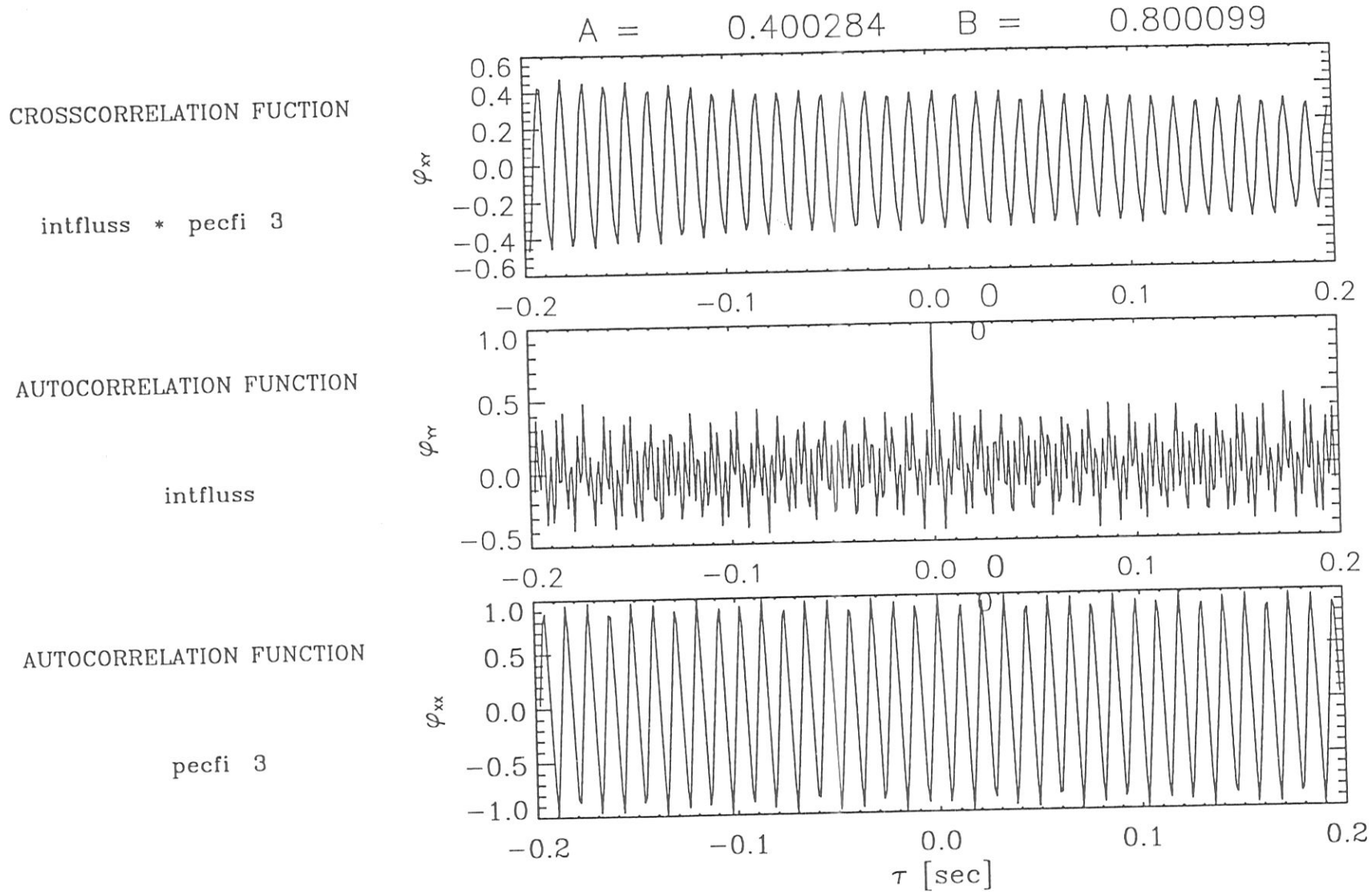

Fig.14: ECRH power modulation in Hydrogen discharge #23664. Correlation

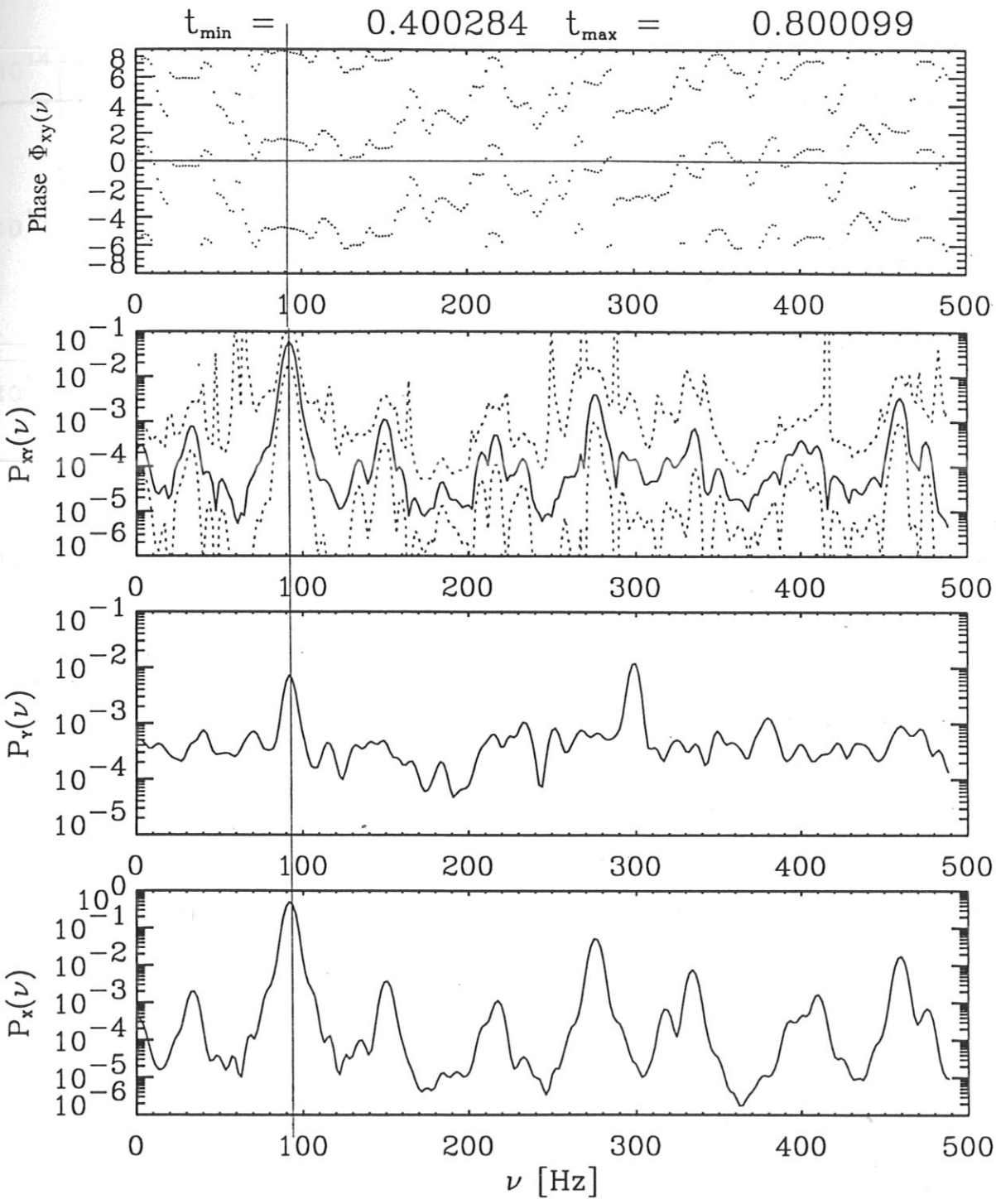

Fig.15: Fourier analysis of discharge #23664 (see Fig.14). The spectral densities $P_x(\nu)$ of the ECRH power and $P_y(\nu)$ of Γ, their cross-spectral density $P_{xy}(\nu)$, and the phase $\Phi_{xy}(\nu)$ between the two.

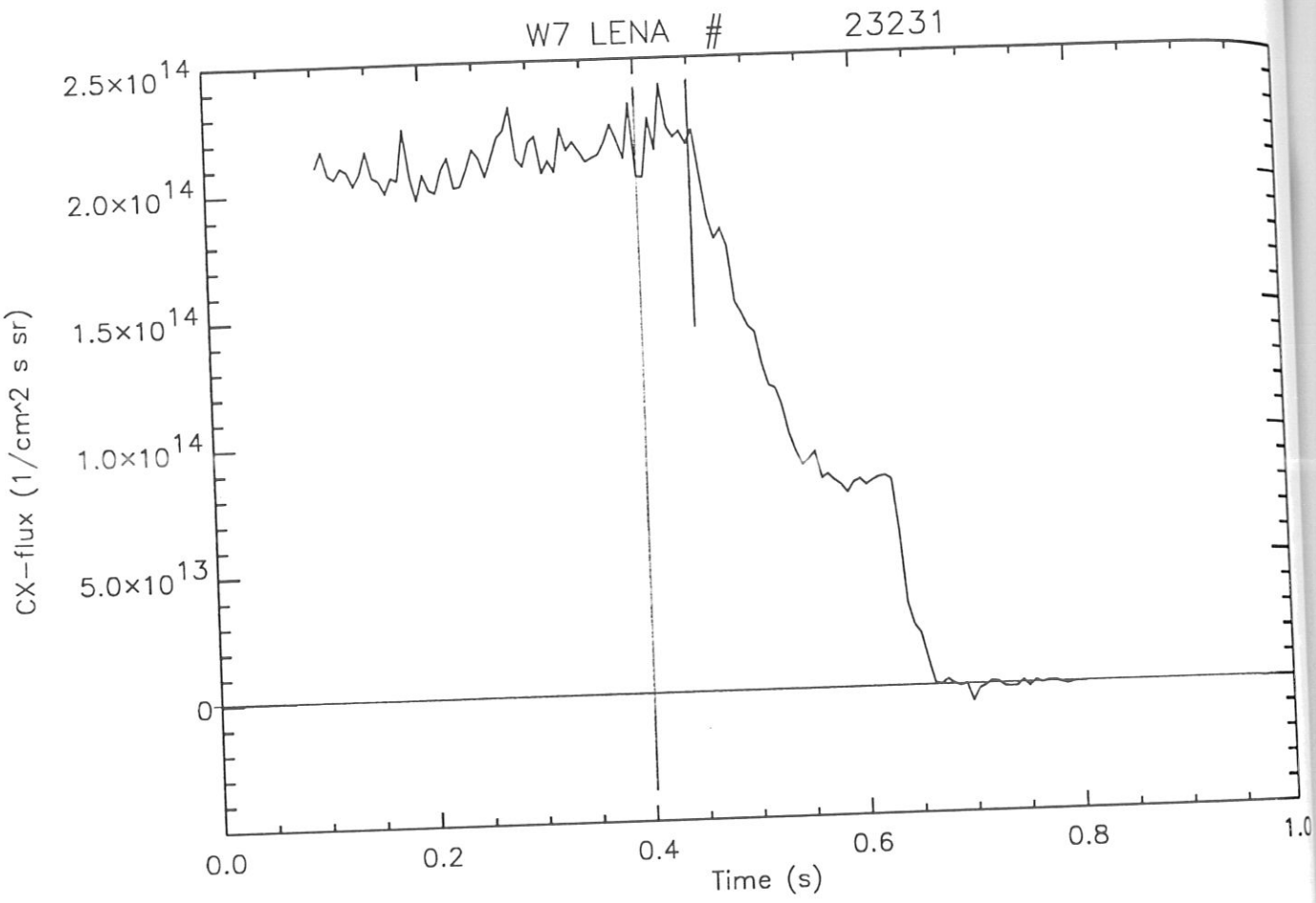

Fig.16: Decay of Γ after closing the external gas valve at 0.4 s.

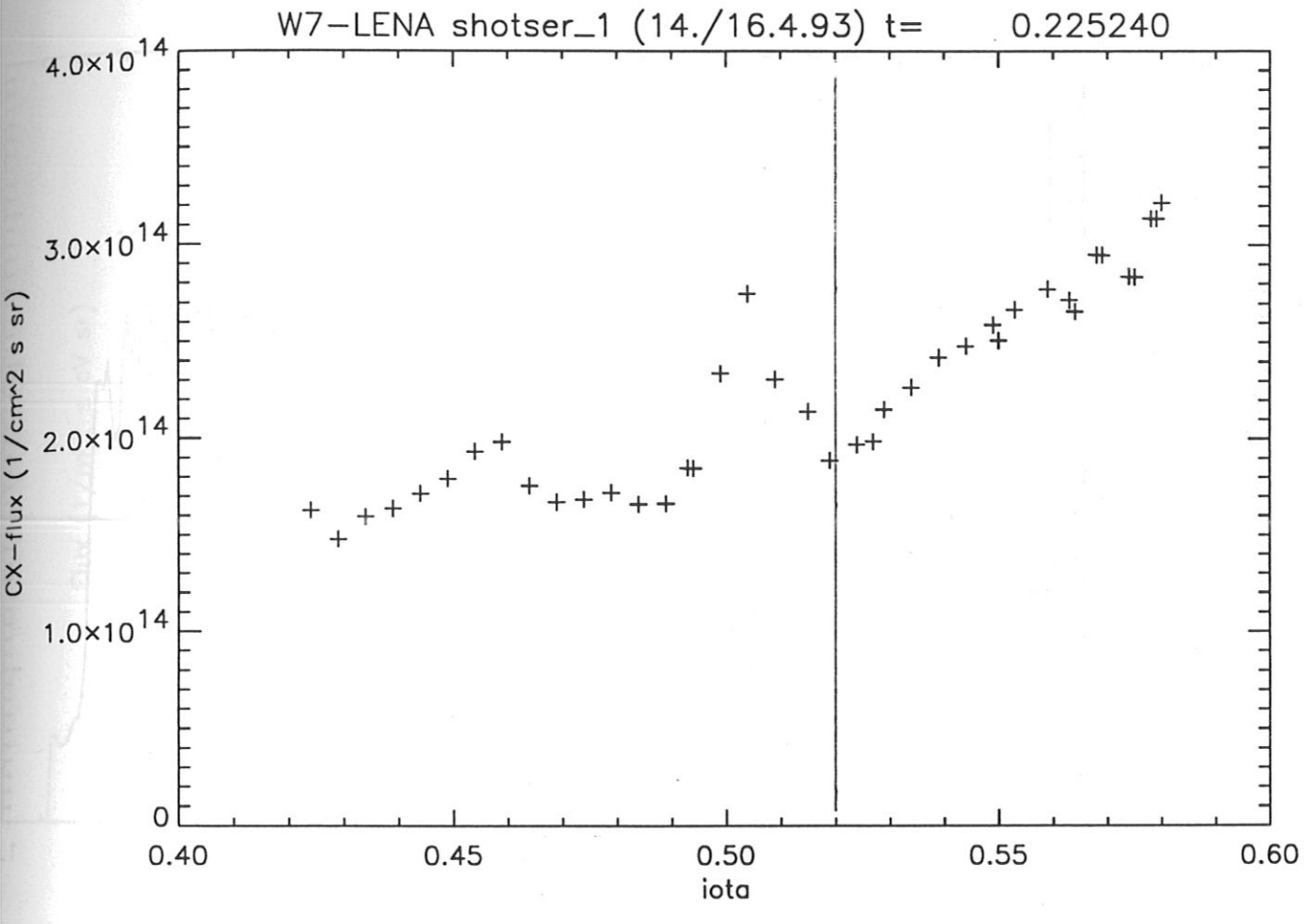

Fig.17: Variation of Γ with iota.

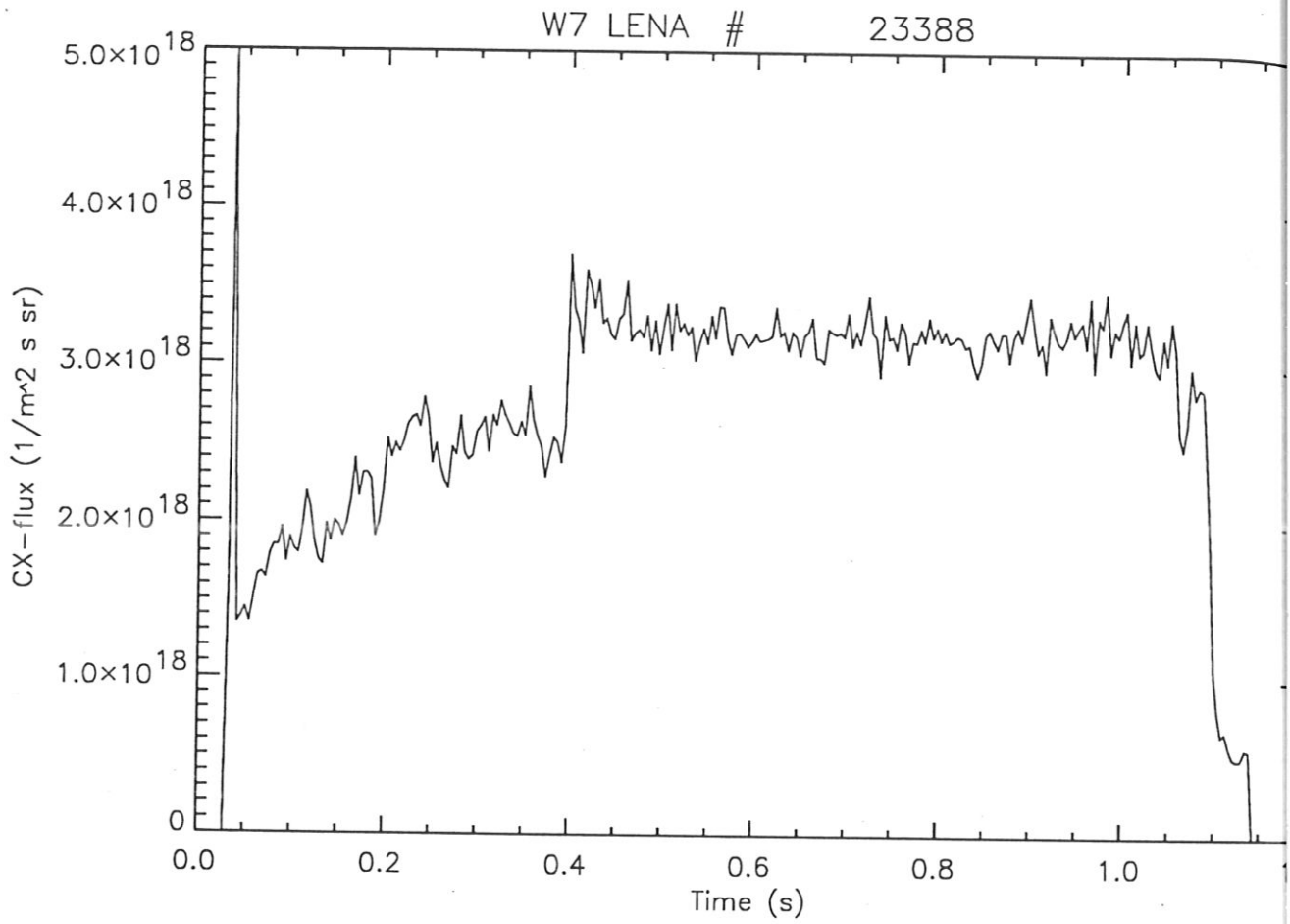

Fig.18: Time dependence of Γ during #23388 with increasing iota. At 0.4 s iota crosses the value of $\iota = 0.5$.

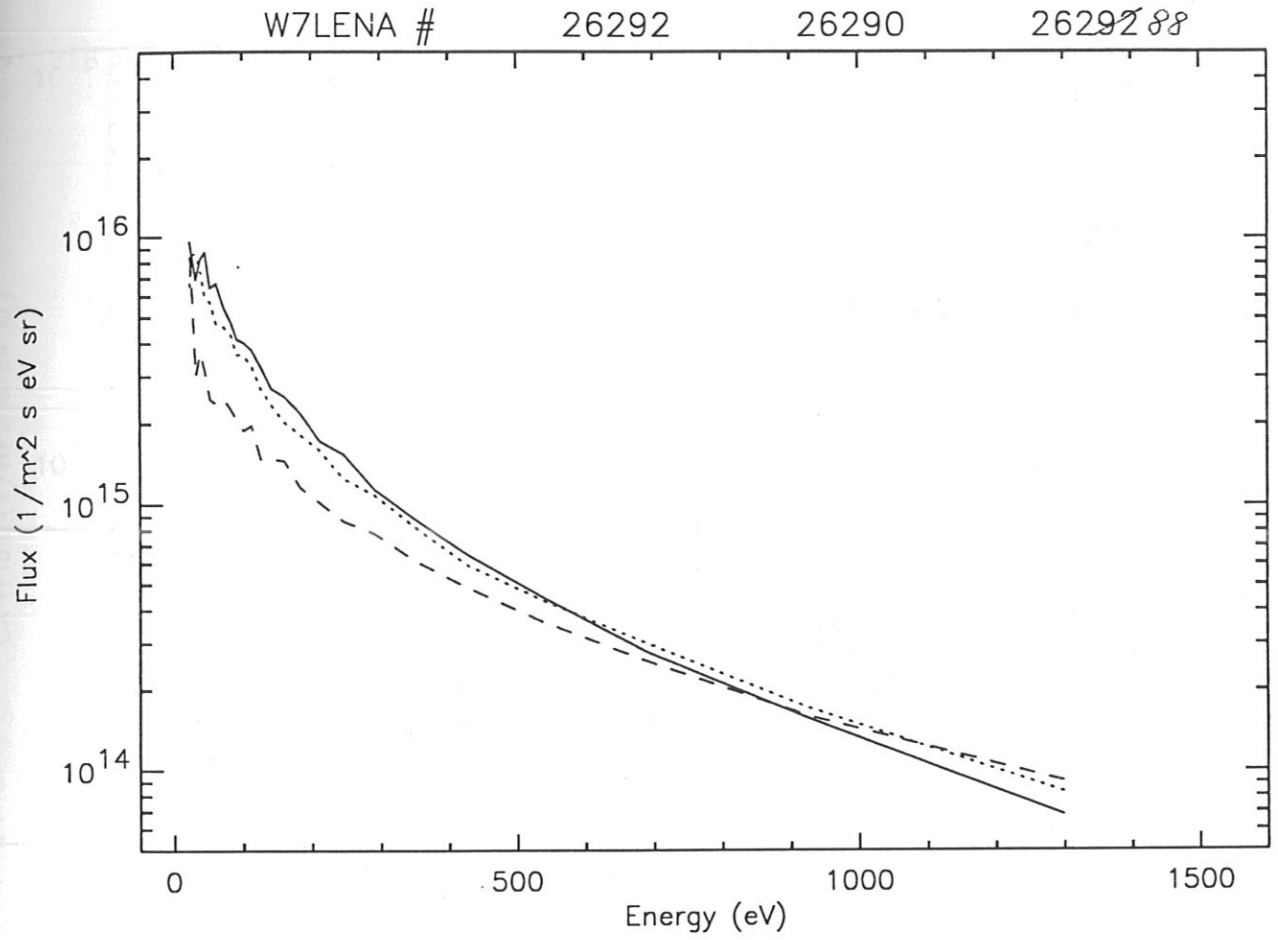

26292 Bt = 1.40T (solid)

26290 Bt = 1.90T (dotted)

26288 Bt = 2.51T (dashed)

Fiig.19: CX-spectra of 3 NBI heated discharges with different values of B_t started with nonresonant 900 MHz radiation.

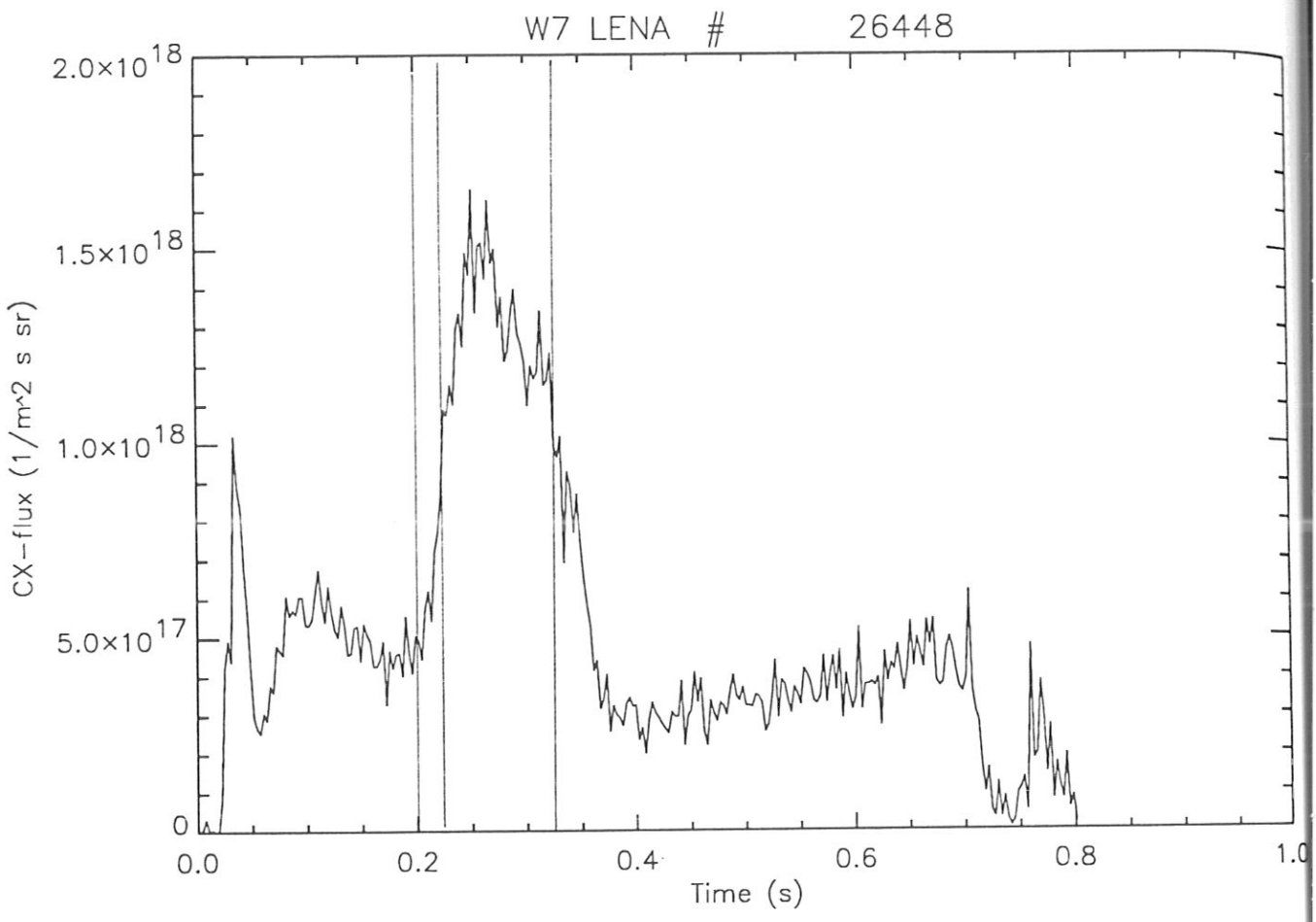

Fig.20: Γ during #26448. 400 kW 70 GHz ECRH 0 to 0.22 s, 880 kW NBI 0.2 to 0.7 s, 720 kW 140 GHz ECRH 0.22 to 0.32 s.

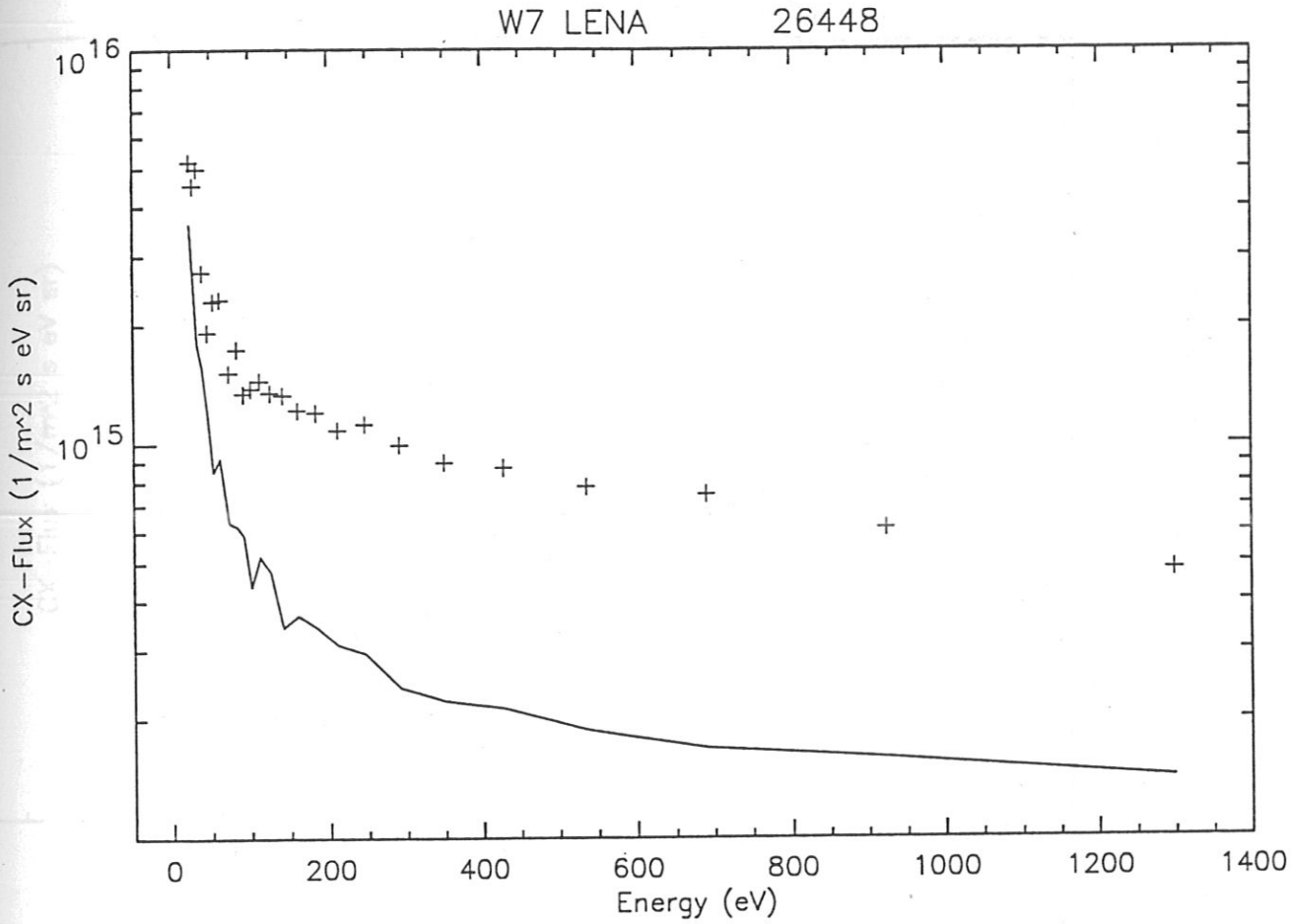

Fig.21: CX-spectra of #26448 (see Fig.20) for NBI (solid line) and for NBI + 140 GHz ECRH (+++).

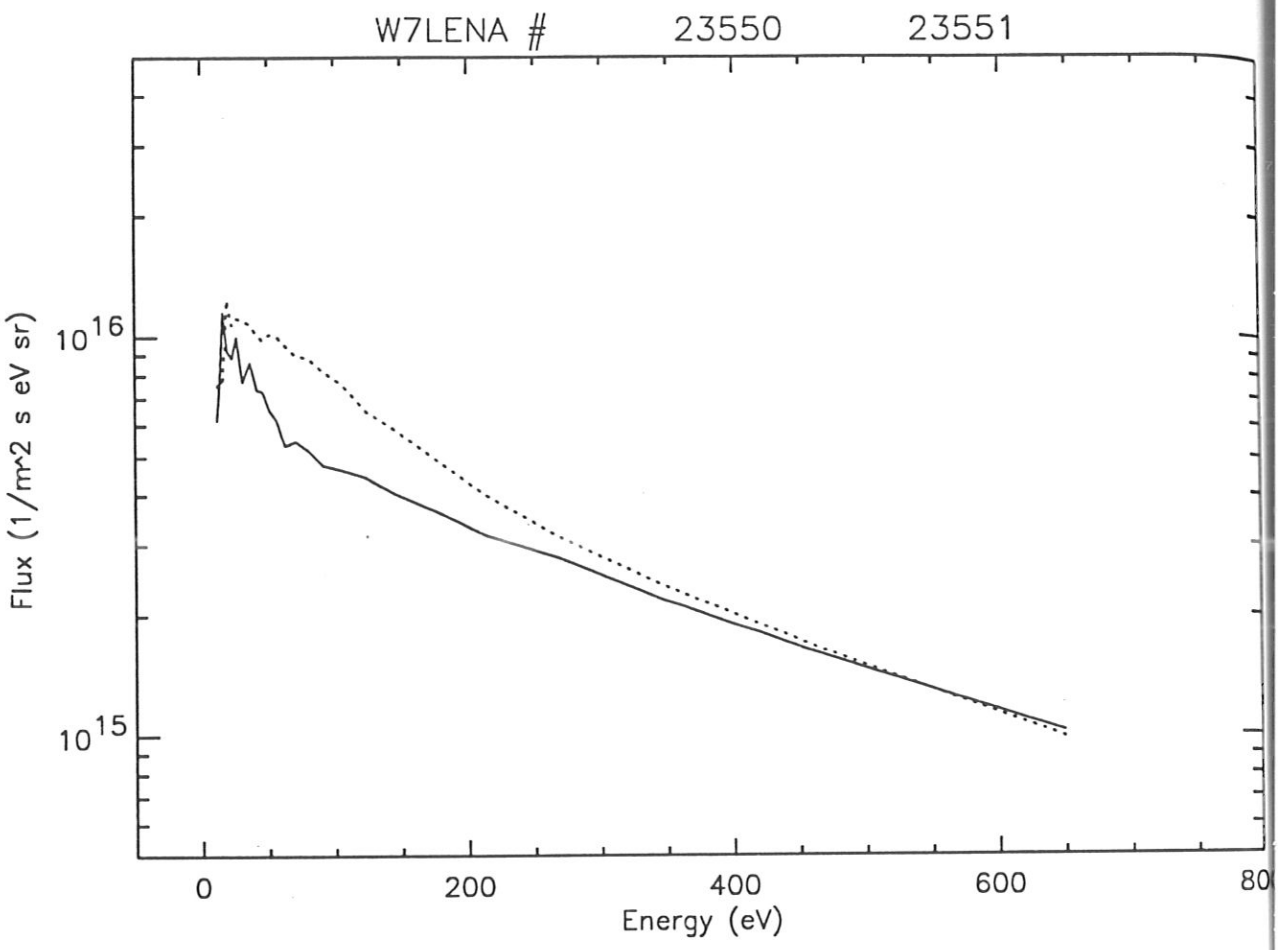

Fig.22: CX-spectra of #23550 at ι = 0.529 (solid line) with H-mode and #23551 at ι = 0.534 (dotted) with no H-mode.

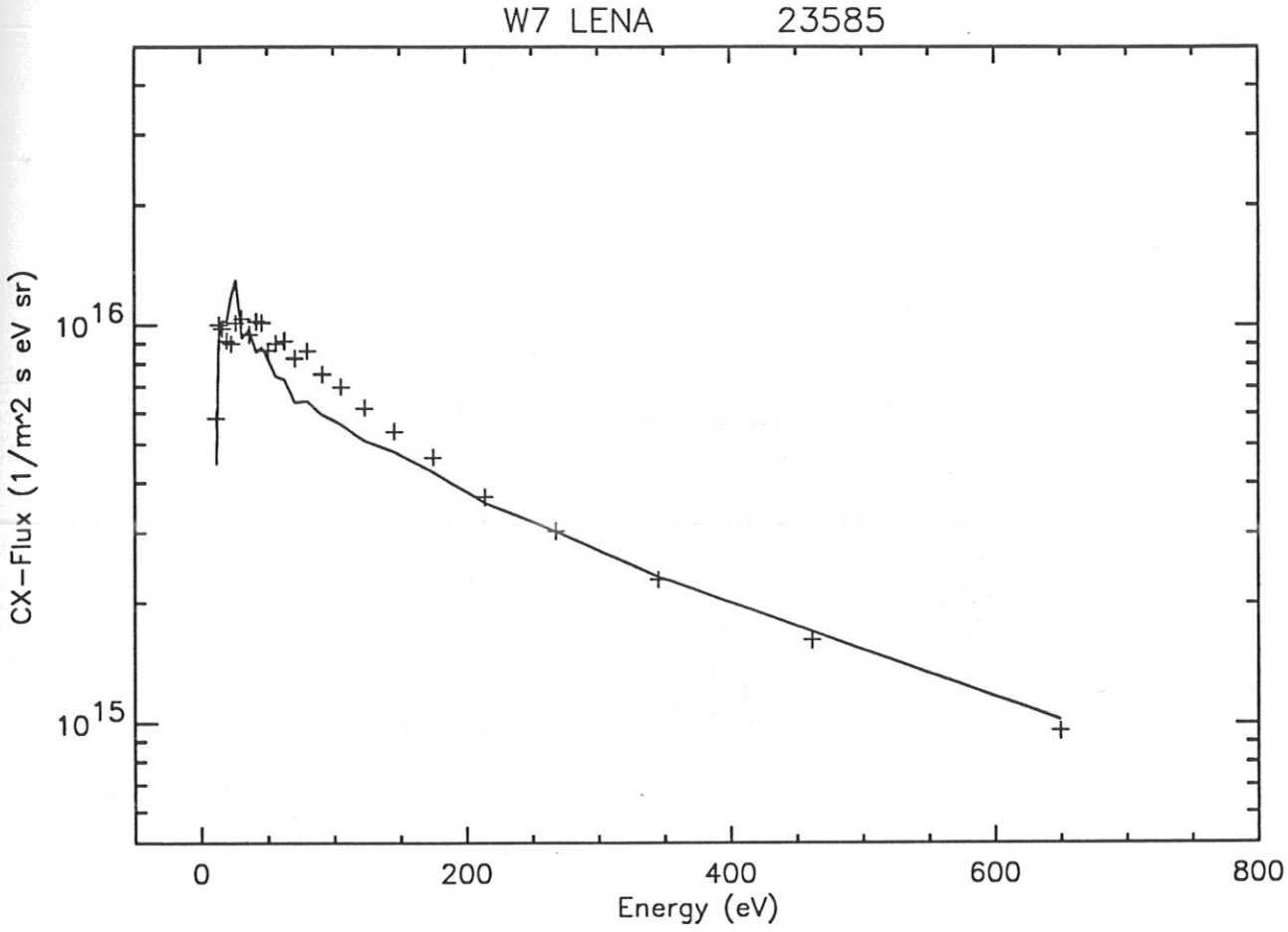

Fig.23: CX-spectra of #23585 before (+++) and after (solid line) the H-mode transition.

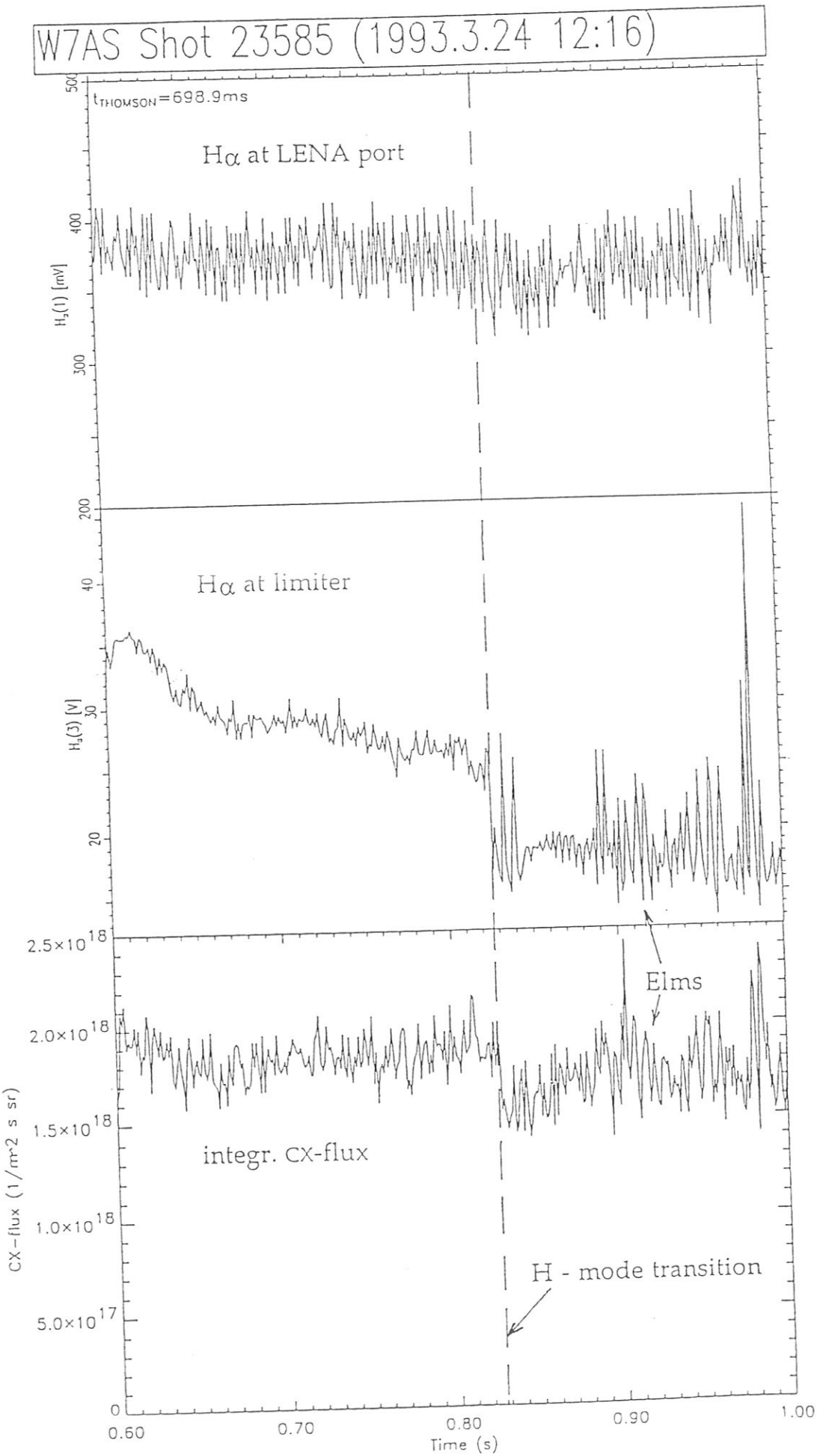

Fig.24: Time dependence of the H_α−signals from the LENA port and the limiter and the CX-flux Γ during #23585 with a H-mode transition at 0.828 s.

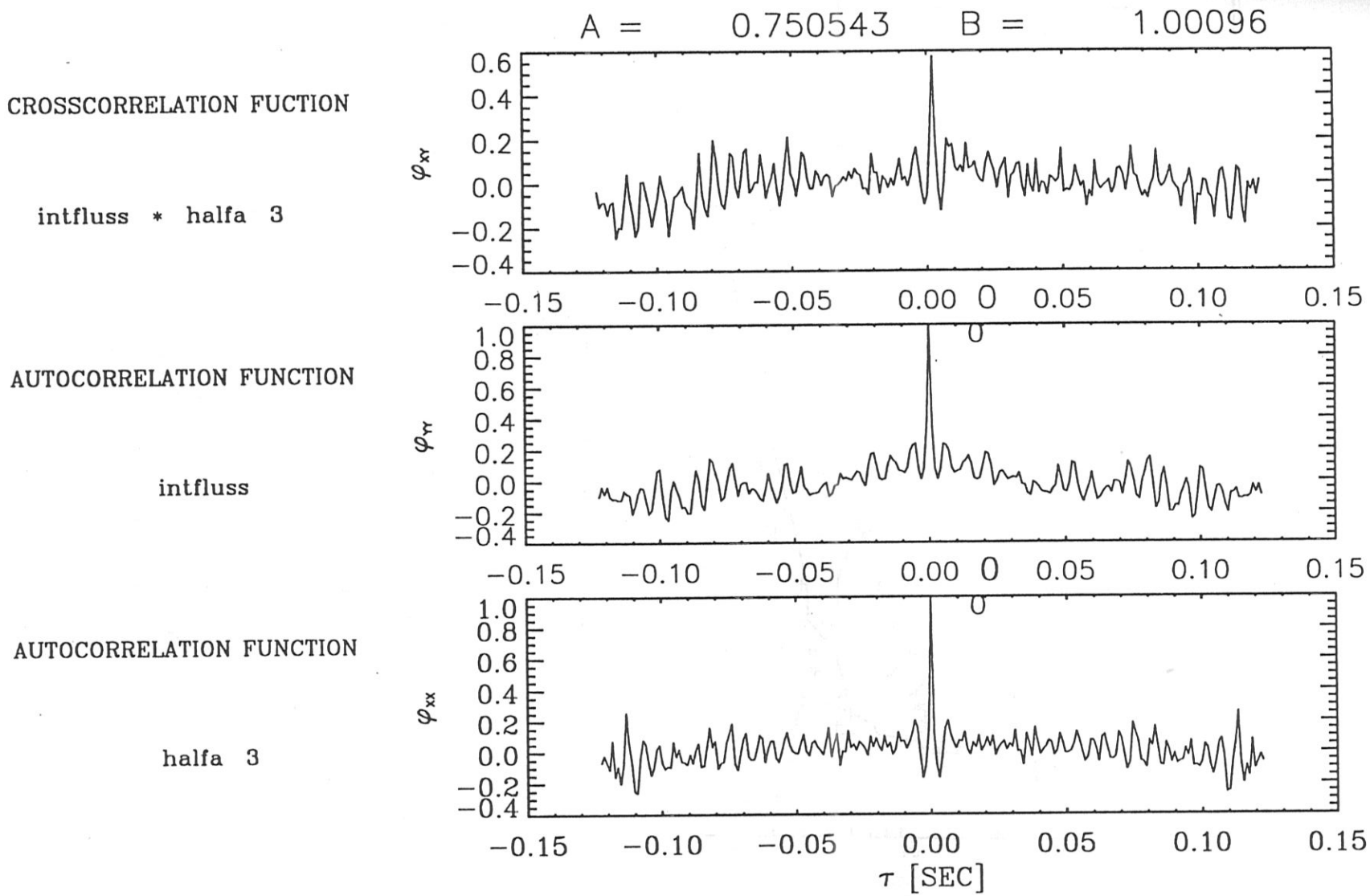

Fig.25: Correlation of Γ and H_α−signal from the limiter ("halfa 3") for shot #23585 (see Figs.23,24).

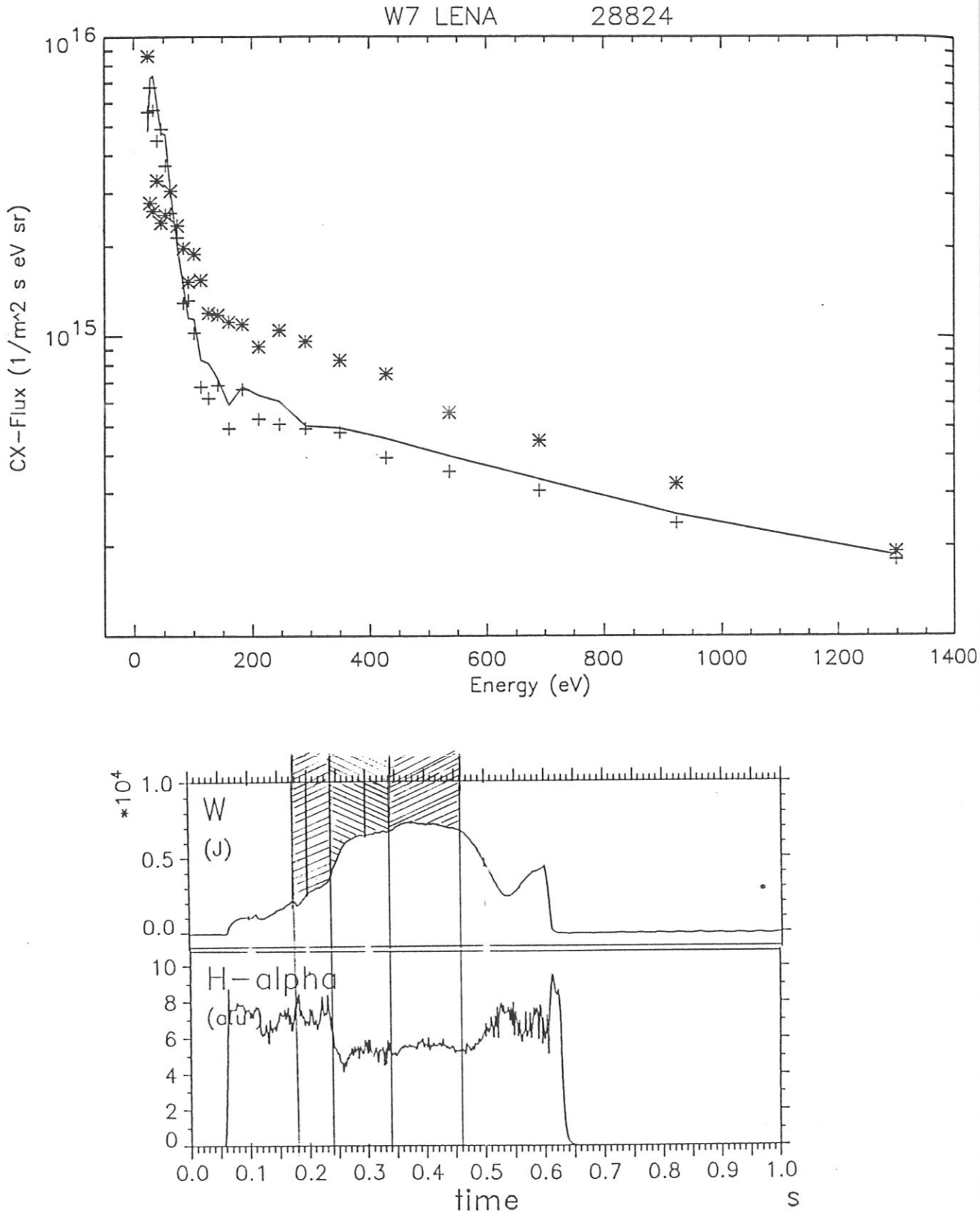

Fig.26: Cx-spectra during #28824 with ι = 0.341, B_t =1.27 T and 840 kW NBI heating. In the lower part the time dependence of W (energy content) and the H_α-signal from the limiter are shown. The spectra are taken during the indicated times with *** 1st interv., +++ 2nd interv., and solid line 3rd interval.

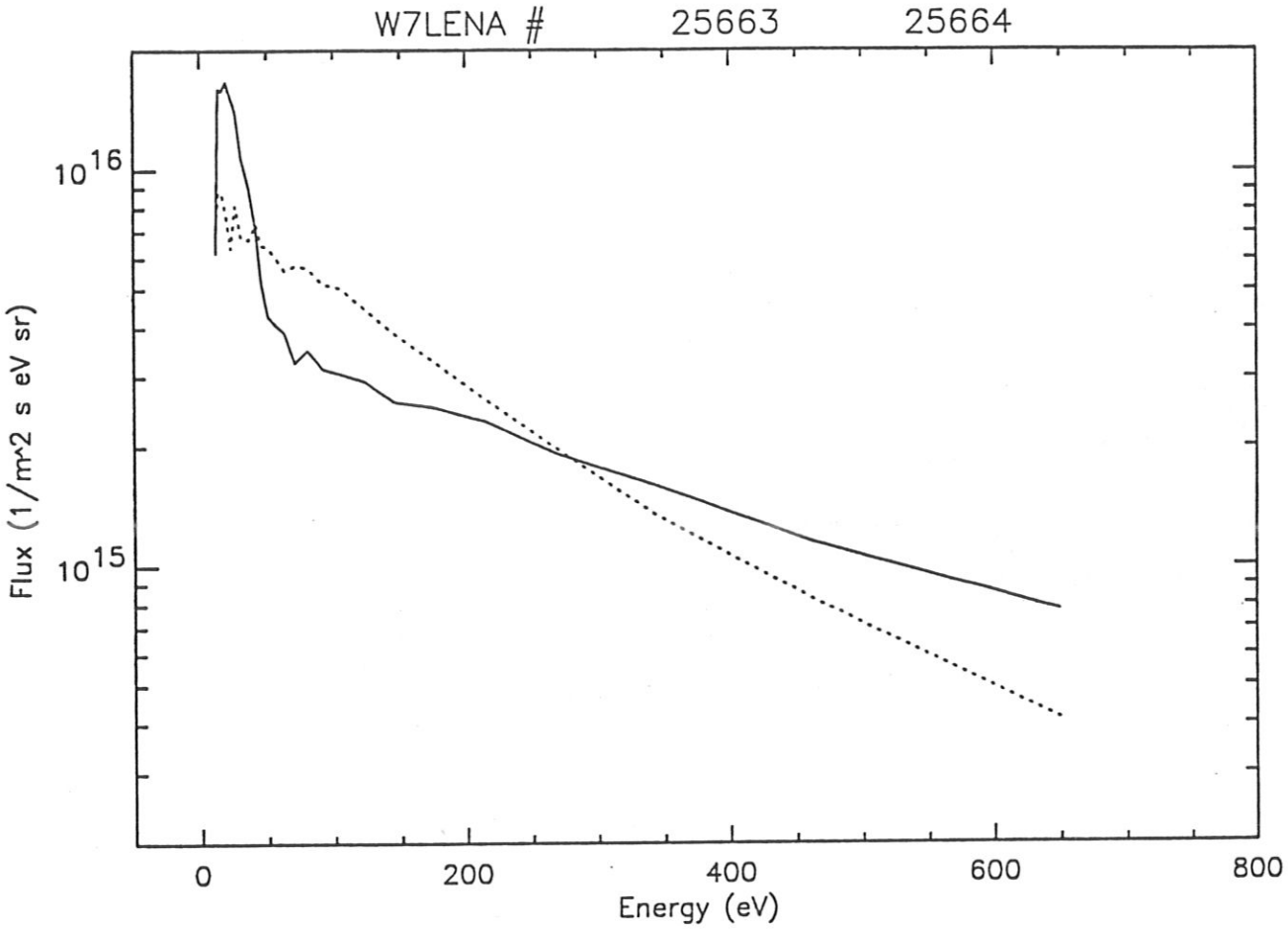

Fig.27: CX-spectra of Hydrogen shots with B_t = 1.21 T and 840 kW NBI heating.

#25663, ι = 0.346 H-mode?? (solid line) and #25664, ι = 0.361 (dotted).